



Mitochondrial dysfunction and autophagy activation are associated with cardiomyopathy developed by extended methamphetamine self-administration in rats

Chowdhury S. Abdullah^{a,1}, Naznin Sultana Remex^{b,1}, Richa Aishwarya^{a,1}, Sadia Nitu^a, Gopi K. Kolluru^a, James Traylor^a, Brandon Hartman^a, Judy King^a, Mohammad Alfrad Nobel Bhuiyan^c, Nicole Hall^d, Kevin Sean Murnane^{d,e}, Nicholas E. Goeders^d, Christopher G. Kevil^{a,b}, A. Wayne Orr^{a,b}, Md. Shenuarin Bhuiyan^{a,b,*}

^a Department of Pathology and Translational Pathobiology, Louisiana State University Health Sciences Center-Shreveport, Shreveport, LA, 71103, USA

^b Department of Molecular and Cellular Physiology, Louisiana State University Health Sciences Center-Shreveport, Shreveport, LA, 71103, USA

^c Department of Medicine, Division of Clinical Informatics, Louisiana State University Health Sciences Center-Shreveport, Shreveport, LA, 71103, USA

^d Department of Pharmacology, Toxicology and Neuroscience, Louisiana State University Health Sciences Center-Shreveport, Shreveport, LA, 71103, USA

^e Department of Psychiatry, Louisiana State University Health Sciences Center-Shreveport, Shreveport, LA, 71103, USA

ARTICLE INFO

Keywords:

Self-administration

Methamphetamine

Cardiomyopathy

Fibrosis

Mitochondrial dysfunction

ABSTRACT

The recent rise in illicit use of methamphetamine (METH), a highly addictive psychostimulant, is a huge health care burden due to its central and peripheral toxic effects. Mounting clinical studies have noted that METH use in humans is associated with the development of cardiomyopathy; however, preclinical studies and animal models to dissect detailed molecular mechanisms of METH-associated cardiomyopathy development are scarce. The present study utilized a unique very long-access binge and crash procedure of METH self-administration to characterize the sequelae of pathological alterations that occur with METH-associated cardiomyopathy. Rats were allowed to intravenously self-administer METH for 96 h continuous weekly sessions over 8 weeks. Cardiac function, histochemistry, ultrastructure, and biochemical experiments were performed 24 h after the cessation of drug administration. Voluntary METH self-administration induced pathological cardiac remodeling as indicated by cardiomyocyte hypertrophy, myocyte disarray, interstitial and perivascular fibrosis accompanied by compromised cardiac systolic function. Ultrastructural examination and native gel electrophoresis revealed altered mitochondrial morphology and reduced mitochondrial oxidative phosphorylation (OXPHOS) super-complexes (SCs) stability and assembly in METH exposed hearts. Redox-sensitive assays revealed significantly attenuated mitochondrial respiratory complex activities with a compensatory increase in pyruvate dehydrogenase (PDH) activity reminiscent of metabolic remodeling. Increased autophagy flux and increased mitochondrial antioxidant protein level was observed in METH exposed heart. Treatment with mitoTEMPO reduced the autophagy level indicating the involvement of mitochondrial dysfunction in the adaptive activation of autophagy in METH exposed hearts. Altogether, we have reported a novel METH-associated cardiomyopathy model using voluntary drug seeking behavior. Our studies indicated that METH self-administration profoundly affects mitochondrial ultrastructure, OXPHOS SCs assembly and redox activity accompanied by increased PDH activity that may underlie observed cardiac dysfunction.

1. Introduction

Methamphetamine (METH) is a highly addictive psychostimulant

drug [1–3]. METH addiction is a growing worldwide health crisis, especially in the United States, due to its ease of illicit manufacturing, increased purity, and availability to people susceptible to addiction

* Corresponding author. Department of Pathology and Translational Pathobiology, and Department of Molecular and Cellular Physiology, Louisiana State University Health Sciences Center, PO Box 33932, Shreveport, LA, USA.

E-mail address: shenu.bhuiyan@lsuhs.edu (Md.S. Bhuiyan).

¹ These authors contributed equally.

<https://doi.org/10.1016/j.redox.2022.102523>

Received 11 October 2022; Accepted 23 October 2022

Available online 1 November 2022

2213-2317/© 2022 The Authors. Published by Elsevier B.V. This is an open access article under the CC BY-NC-ND license (<http://creativecommons.org/licenses/by-nc-nd/4.0/>).

[4–6]. METH use has been implicated as a causal factor of vital organ and tissue systems failure in the body. Notably, cardiovascular diseases underlie the second leading cause of death in people who use METH following accidental overdose [2,7]. METH addiction profoundly affects the cardiovascular system, causing acute and chronic effects, including acute sinus tachycardia, acute coronary vasospasm, pulmonary arterial hypertension, acute myocardial infarction, myocardial ischemia, and cardiomyopathy [2,8–14]. Remarkably, cumulative case-control studies consistently reported clinical pathologies of METH-associated cardiomyopathy in patients who use METH with a significantly increased prevalence of heart failure with chronic METH use [9,11,15–18]. METH-associated cardiomyopathy has been clinically presented with right and left ventricular (LV) chamber dilations, cardiac hypertrophy, severely reduced LV percent ejection fractions (LVEF), and heart failure (HF) in individuals who use METH [9,15–17]. Notably, independent studies showed compromised LVEF in even young people who use METH irrespective of sex, race, and other common cardiovascular risk factors [15,19–22]. Cellular and molecular characteristics of METH-associated cardiomyopathy in humans are characterized by myocardial lesions, necrotic foci, ischemia, myocardial immunogenicity, signs of inflammation, and extensive perivascular and interstitial fibrosis [11,15,23]. In addition, METH-cardiomyopathy patients also exhibit a correlation between the extent of cardiac fibrosis to the severity of cardiac ejection fractions decline [15]. Despite the well-documented adverse effects of chronic use of METH on the human heart, there are currently no FDA-approved drugs available to treat either METH use disorder or METH-induced cardiomyopathy people suffering from addiction, leaving them with few options, such as cognitive and behavioral therapies to thwart METH addiction.

There is a scarcity of scientific reports on deciphering molecular mechanisms responsible for the development of METH-induced cardiac dysfunctions. Among the reported events associated with METH treatment in rodent hearts, the most common pathological changes include increased reactive oxygen species (ROS) generation, mitochondrial dysfunctions, impaired calcium dynamics, altered gene expressions, augmented inflammation, abnormal myocardial lesions, cardiomyocytes apoptosis, and necrosis [23–30]. The majority of these research on the effects of METH on the heart were cursory reports involving studies on the effects of acute toxic doses of METH administration [24,27,31]. However, a more realistic representation of the use of METH in people afflicted with METH addiction is ‘binge and crash’ which is characterized by long, repeated binges of METH use, often without food or sleep, followed by periods of abstinence or sleep, often referred to as a crash [32–34]. Recent development of a rodent model which more closely resembles aspects of human METH use allows for extended access self-administration of METH resulting in an escalation of drug intake and brain METH levels in rats comparable to that of people chronically using METH [35–38]. Therefore, the aim of the present study was to determine the molecular, functional, and pathological events associated with the development of cardiomyopathy in the model of rodent self-administration of METH. In the present study, we have utilized our previously reported METH self-administered rat models mimicking the human METH addiction pattern to determine the molecular events associated with METH cardiomyopathy using integrated and complementary gravimetric, morphometric, histological, gene expression, and longitudinal echocardiographic studies [35,38,39]. We employed transmission electron microscopic observations, electron transport system, metabolic and autophagy process associated proteins expression analysis, native gel electrophoresis, and enzymatic metabolic assays to dissect molecular underpinnings associated with the development of METH-cardiomyopathy following self-administration of METH in rats.

2. Materials and methods

2.1. Data availability and disclosure statement

The authors declare that all supporting data and method descriptions are available within the current article or from the corresponding author upon reasonable request.

2.2. Animals

We have used 80–100 days old adult male and female Wistar rats (Harlan Sprague Dawley, Indianapolis, IN). Both control and METH self-administration rats were free-fed until they reached a minimum body weight of 390 g for males and 290 g for females. The rats were then maintained at 85–90% of their free-feeding body weights (approximately 330 g for males and 245 g for females) with free access to water, as reported earlier [35,38]. The rats were fed once per day in the self-administration chamber similar to that while in their home cages (14 g of food, standard rodent chow, Harlan Teklad, Madison, WI, USA). A chronic indwelling jugular catheter was implanted in METH and Control rats and allowed a minimum of five days to recover following surgical procedures. Each rat was singly housed in cages equipped with a laminar airflow unit and air filter in an AALAC-accredited animal care facility. We have also acquired timed pregnant female Sprague-Dawley rats from Charles River Laboratories (Portage, MI) to isolate primary neonatal rat cardiomyocytes (NRCs) from newborn rat pups [23,40]. All animals were handled and cared for according to the Guide for the Care and Use of Laboratory Animals: Eighth Edition (National Institutes of Health, Bethesda, MA). All experiments involving animals were approved by the Institutional Animal Care and Use Committee of LSU Health Sciences Center-Shreveport.

2.3. METH self-administration protocol

Each rat was implanted with a chronic indwelling jugular catheter to intravenously self-administer METH as described previously [35,37,38,41]. Control rats were paired with METH rats in a yoked saline control paradigm. Rats were put in the operant chambers to receive METH or saline through a self-administration milieu. Briefly, Tygon tubing covered with a protective spring leash was attached to the catheter. The Tygon tubing was further connected to a dual channel fluid swivel (Instech, Plymouth Meeting, PA) located at the top of the chamber and continued outside of the chamber to a 60 mL syringe contained in a motor-driven pump. Each experimental chamber contained two response levers mounted on one wall of the chamber, and a stimulus light was located above each lever. METH rats were trained to self-administer METH by pressing one of the response levers (i.e., the “active” lever) under a fixed-ratio 1 (FR1) reinforcement schedule [38]. Depression on the inactive lever resulted in no programmed consequences. The weekly METH self-administration session began on Mondays at around 11:00 a.m. and ended on Fridays at around 11:00 a.m. At the beginning of the session, a stimulus light was illuminated above the active lever to indicate the availability of METH. One depression of the active lever by rats resulted in an intravenous infusion of METH dissolved in 0.9% heparinized sodium chloride at a dose of 0.06 mg/kg/infusion in 50 μ L over 0.83 s. There was a 20-s timeout period following each infusion. The stimulus light above the active lever was extinguished during the infusion and the timeout period, and illuminated again once the timeout ended. Since the body weight of the rats was stable (approximately 85% of their free-feeding body weights) through our feeding regime, the rats received METH based on their body weight throughout the study period. When the METH rat received an infusion, the yoked saline control partner simultaneously received an infusion of 50 μ L of 0.9% heparinized sodium chloride intravenously. Depression of the active and inactive levers in the saline control boxes resulted in no programmed consequences. Following completion of the

96-h METH self-administration session on Friday mornings, the rats were placed into their home cages for the next 72 h without access to METH. The 96-h METH self-administration sessions were resumed on the following Monday at around 11:00 a.m. All the rats were completed 8 consecutive weeks under this protocol [35,38]. The control and METH self-administered rat cohorts were then subjected to an array of complimentary experiments as described below.

2.4. Gravimetric and morphometric analyses

Whole rat hearts were excised from the euthanized animals and wet heart weights were measured on an OHAUS electronic balance machine (NJ, USA). Heart gravimetric indices were determined by calculating heart weight (mg)-to-body weight (g) ratios and heart weight (mg)-to-tibia length (cm) ratios. To assess cardiomyocytes cross-sectional areas, formalin fixed, paraffin embedded 5 μm thick rat heart LV tissue sections were deparaffinized, hydrated, heat-induced antigen retrieved and stained with Alexa Fluor 488 Wheat Germ Agglutinin (5 $\mu\text{g}/\text{mL}$, Invitrogen) for 1 h at room temperature (RT). 4',6-diamidino-2-phenylindole (DAPI, Invitrogen) was used to counterstain nuclei [23,42,43]. We used Nikon A1R high-resolution confocal microscope (Nikon Instruments inc., Melville, NY) coupled with Nikon NIS Elements Software (v4.13.04) to image the stained tissue sections on a 60 \times oil objective lens (NA = 1.4). Cardiomyocytes cross sectional areas (μm^2) were measured in an analyst-blinded manner on alphanumerically labeled images using NIH ImageJ software (Bethesda, MD) [23].

2.5. Tissue histology

Formalin fixed, paraffin embedded 5 μm thick rat heart LV tissue sections were deparaffinized, hydrated and stained with Picosirius Red (PSR) and Masson's Trichrome to determine collagen deposition and percent fibrotic areas, respectively [23]. Heart tissue sections were also stained with Hematoxylin and Eosin (H&E) staining kit (H-3502, Vector Laboratories) according to the manufacturer's instructions to assess cardiac structural integrity and histology. Alphanumerically labeled stained heart tissue sections were imaged at brightfield using an Olympus BX40 microscope (Feasterville, PA) on 10 \times objective lens in an investigator-blinded manner. Percent collagen deposition areas (stained in red with PSR) and percent fibrotic areas (stained blue with Trichrome) relative to total stained myocardium areas (μm^2) in each microscopic field were quantified on NIH ImageJ (v1.6.0) software (Bethesda, MD) [23,42]. Randomly 8–10 high magnification microscopic fields from LV were analyzed in stained rat heart sections.

2.6. Transmission electron microscopy

Control and METH self-administered rat LV heart sections were fixed with 2% glutaraldehyde and post-fixed with 1% OsO₄. Multiple thin sections were cut in 100 nm thickness using an ultramicrotome, followed by counterstaining with uranium and lead salts. The stained LV sections were examined under a JEOL 1400 120 kV transmission electron microscope (Peabody, MA) equipped with an AMT digital camera [23,42,44]. We used two control and two METH self-administered rat LV heart sections to assess cardiac ultrastructure.

2.7. Echocardiography

Transthoracic longitudinal M-mode echocardiography LV traces of isoflurane-anesthetized Control and METH self-administered rats were detected using a 40-MHz transducer and imaged using VisualSonics Vevo 3100 high-resolution micro-ultrasound imaging system (FUJIFILM, Toronto, ON, Canada) coupled with Vevo LAB 3.1.1 imaging software (VisualSonics, Toronto, ON, Canada) [23,40,42,43]. Parasternal short axis 2D M-mode images were analyzed using Vevo LAB software (v5.5.0) to quantify LV structural and functional indices,

including LV systolic and diastolic volume (LV Vol; s and LV Vol; d, respectively), LV internal diameter at systole and diastole (LVID; s and LVID; d, respectively), interventricular septum thickness at systole and diastole (IVS; s and IVS; d, respectively), and LV posterior wall thickness at systole and diastole (LVPW; s and LVPW; d, respectively). Cardiac systolic functional parameters percent fractional shortening (%FS) were calculated as $\%FS = (LVID; d - LVID; s) / LVID; d \times 100$ and percent ejection fraction (%EF) were calculated as $\%EF = (LV Vol; d - LV Vol; s) / LV Vol; d \times 100$ in control and METH self-administered rats [23].

2.8. Primary cardiomyocytes isolation

Primary neonatal rat ventricular cardiomyocytes (NRCs) were isolated from 1- to 2-day old Sprague-Dawley rat pups [23,40,44–46]. The dissected rat pup heart ventricles were subjected to sequential enzymatic digestion with collagenase II (Worthington) and Trypsin (Gibco). Fibroblasts were removed from the cell isolates through a pre-plating step. Next, cardiomyocytes were counted and plated at 1.5×10^6 cells per 10 cm^2 plates in culture media containing 10% fetal bovine serum (FBS, Gibco), 1% antibiotic-antimycotic mixture (Gibco) in α MEM media (Gibco). After 24 h, culture media was changed to DMEM (Gibco) containing 2% FBS and 1% antibiotic-antimycotic. Afterwards, cardiomyocytes were subjected to saline or METH at specified concentrations and time points. Assessment of autophagic flux in METH treated cardiomyocytes was performed by measuring the LC3B II protein levels with and without lysosomal inhibition as described previously [40,47]. To inhibit lysosomal function, media containing 50 nmol/L Bafilomycin A1 (Sigma) was added to the cells for 3 h. To inhibit cellular autophagosomes synthesis, cell culture media were supplemented with PI3K inhibitor Wortmannin (W1628, Millipore-Sigma) at a final concentration of 1 μM for 3 h dissolved in DMSO. To quench mitochondria-derived reactive oxygen species, MitoTEMPO (SML0737, Sigma), a mitochondria-targeted antioxidant, dissolved in DMSO was added to cell culture media at 5 μM and 10 μM final concentrations to cardiomyocytes. In all cell culture experiments, vehicle cardiomyocytes received either an equal volume of saline (METH dissolution media) and/or received an equal volume of DMSO (BafA1, Wortmannin dissolution media), where appropriate.

2.9. siRNA transfection in cardiomyocytes

To genetically knockdown of Atg7, cardiomyocytes were transfected with Atg7 siRNA (CCAGUCUGUUGAAGUUCUCUGUUU and AAAGCAGAGAACUUCACAGACUGG; Invitrogen) using Lipofectamine 2000 (Invitrogen) in Opti-MEM reduced serum medium (Invitrogen) for 16 h [23,45–47]. After 16 h of incubation, media were changed to regular culture media containing 2% FBS [23,45–47]. A non-specific siRNA was used as a negative control in all gene silencing experiments.

2.10. Western blot

Rat left ventricular heart tissues and neonatal rat cardiomyocytes (NRCs) were lysed with ice-cold Cell Lytic M buffer (Sigma-Aldrich) containing 1x Halt protease and phosphatase inhibitor cocktail (Invitrogen) [23,40,44,45,47,48]. The lysed cell materials were sonicated briefly followed by centrifugation at 14,000 \times g for 15 min to precipitate insoluble cell debris. The protein concentrations of NRC lysate supernatants were quantified using the modified Bradford reagent (Bio-Rad) relative to a bovine serum albumin standard curve (Bio-Rad). Equal concentrations of protein were used to prepare samples with 6 x Laemmli's sample buffer for western blot experiments. Subsequently, equal amounts of protein (20–30 μg) were resolved on sodium dodecyl sulfate polyacrylamide 7.5–12% gels and transferred to polyvinylidene difluoride (PVDF) membranes (Bio-Rad). Membranes were then blocked with 5% non-fat skim milk and incubated with primary antibodies overnight. The following primary antibodies were used for

immunoblotting: LC3B (1:1000, 2775, Cell Signaling), p62 (1:500, GP62-C, Progen), Cathepsin D (1:1000, sc-6487, Santa Cruz), Beclin1 (1:1000, sc-10086, Santa Cruz), MnSOD (1:1000, 06-984, Millipore-Sigma), SOD1 (1:1000; 37385, Cell Signaling), Catalase (1:1000, 12980, Cell Signaling), Glutathione peroxidase 1 (1:1000, ab108427, Abcam) and GAPDH (1:1000, MAB374, EMD Millipore). Subsequently, membranes were washed in 1x TBS-T buffer, probed with alkaline phosphatase-conjugated secondary antibodies (Jackson ImmunoResearch Laboratories, Inc.) at room temperature for an hour, developed using ECF substrate (Amersham), and imaged using a ChemiDoc™ Touch Imaging System (Bio-Rad). Following the transfer, PVDF membranes were probed with Ponceau S to confirm equal protein loading. Densitometric analysis of detected protein bands was quantified using NIH ImageJ software [23].

2.11. Gene expression analysis

Snap-frozen cardiac ventricular samples were subjected to total RNA isolation protocol using RNazol RT (Molecular Research Center, Cincinnati, OH) according to the manufacturer's instructions. Using 5 µg RNA as template, cDNA was synthesized with iScript Advanced cDNA synthesis kit for real-time polymerase chain reaction (RT-PCR) (Bio-Rad, Hercules, CA). Quantitative RT-PCR was run on a CFX96 Touch RT-PCR detection system (Bio-Rad) using Power up SYBR Green Master Mix (A25742, Applied Biosystems, Foster City, CA) for cardiac genes including *Nppa*, *Nppb*, *Myh7*, *Acta2*, *Postn*, *TGFB1*, *TGFB2*, and *TGFB3* as described earlier [23,42,49]. 18S rRNA (Applied Biosystems) was used as a reference gene [50–53]. All samples were run in triplicate wells to calculate the fold change in mRNA expression using the comparative Ct method [$2^{-(\Delta\Delta Ct)}$]. Expression values were averaged and expressed as the fold change in mRNA expression in METH-treated rats compared to control rats [23].

2.12. Cardiac mitochondria isolation

Cardiac mitochondria were isolated from the freshly dissected heart ventricles from euthanized rats. Heart ventricles were homogenized in mannitol-sucrose-ethylene glycol tetraacetic acid (EGTA) buffer containing 225 mM mannitol, 75 mM sucrose, 5 mM HEPES, and 1 mM EGTA (pH 7.4) utilizing a hand-held glass/Teflon Potter Elvehjem homogenizer. Next, mitochondria were isolated from the homogenized heart whole cell lysates using differential centrifugation [23,40,42–44]. Fresh mitochondria were subjected to native gel electrophoresis as outlined below. Aliquots of freshly isolated mitochondria were stored at -80°C for mitochondrial complex activity assays.

2.13. Blue native polyacrylamide gel electrophoresis

Freshly isolated cardiac mitochondria were subjected to blue native polyacrylamide gel electrophoresis (BN-PAGE) as described previously [43,54–56]. Briefly, fresh mitochondria were suspended in a solubilization buffer containing 50 mM Bis-Tris (pH 7.0), 1% n-dodecyl- β -d-maltoside (vol/vol), and 750 mM ϵ -amino-N-caproic acid. The suspension was incubated on ice with occasional vortexing for 1 h, followed by centrifugation at 8000g for 10 min. The protein concentration of the supernatant was quantified using the modified Bradford method (Bio-Rad) and mixed with 10x BN-PAGE loading buffer containing 0.5 M ϵ -amino-N-caproic acid and 3% Serva Blue G-250 (wt/vol). Equal amounts of protein were resolved in non-gradient polyacrylamide gels consisting 4% stacking gel and 8% resolving gel. Mitochondrial proteins were resolved at room temperature using gel buffer (500 mM amino-caproic acid and 50 mM Bis-Tris, pH 7.0), cathode buffer (50 mM Tricine, 15 mM Bis-Tris, pH 7.0), 0.02% Serva blue G-250 (wt/vol), anode buffer (50 mM Bis-Tris pH 7.0), and sample buffer (75 mM aminocaproic acid containing 0.3% Serva blue G-250 [wt/vol]). 30 µg proteins were loaded in each lane and run at 150 V until the front blue line had entered

two-thirds of the gel. Next, the cathode buffer was replaced with buffer without Serva blue G-250 (50 mM Tricine, 15 mM Bis-Tris, pH 7.0), and the gel was run at 250 V till the end. BN-PAGE gel was stained with Coomassie blue (BioRad) and imaged on a ChemiDoc Touch Imaging System (Bio-Rad). We further confirmed the specific complexes' subunit localization and relative expression by probing the transferred BN-PAGE gels to PVDF membrane with anti-OXPHOS (1:1000, ab110413, Abcam) primary antibody followed by ECF substrates mediated detection of protein bands on ChemiDoc Touch Imaging System (Bio-Rad) as described above. Briefly, BN-PAGE gels were transferred to PVDF membranes, acid washed to remove Coomassie blue staining, blocked, and probed with anti-OXPHOS cocktail antibodies to detect mitochondrial respiratory chain complex subunits expression.

2.14. PDH activity assay

Pyruvate dehydrogenase (PDH) activity was measured using isolated mitochondria with PDH Activity Assay Kit (MAK183, Sigma-Aldrich) according to manufacturer's instruction. Mitochondria pellets were homogenized in 50 µL of ice-cold PDH assay buffer and centrifuged at $10,000\times g$ for 5 min at 4°C . Supernatants were then subjected to NADH generating reactions in the presence of PDH substrate at 37°C . Absorbance at 450 nm was recorded for 30 min at 1 min interval on CLARIOstar Plus microplate reader (BMG Labtech). PDH activity was measured as rates of NADH production in nanomoles (nmol) per minute per mg of mitochondria using an NADH standard curve (Sigma-Aldrich) [43].

2.15. Citrate synthase activity assay

Citrate synthase activity was measured in isolated mitochondria as reported earlier [43,57]. Briefly, isolated mitochondria were homogenized with Cell-lytic-M (Sigma Aldrich) supplemented with protease inhibitor (Roche). Mitochondrial lysates were incubated with reaction mixture containing 0.2% Triton X-100, 0.31 mM acetyl CoA, and 0.1 mM 5,5'-dithiobis (2-nitrobenzoic acid) (DTNB). The reaction was started by adding 0.5 mM oxaloacetate in 1 mL reaction in a cuvette. Absorbance was recorded at 412 nm at 37°C using DS-11 FX + spectrophotometer (DeNovix). Citrate synthase activity was calculated using $13.6\text{ mM}^{-1}\text{ cm}^{-1}$ as the extinction coefficient value of DTNB and expressed as nmol per minute per mg of mitochondrial protein [57].

2.16. Mitochondrial ETC complex activity assays

We used isolated cardiac mitochondria to measure mitochondrial electron transport chain (ETC) complex activities spectrophotometrically, as described previously [42,43,57]. Total complex I activity was determined by measuring absorbance changes due to NADH (10 µmol/L) oxidation at 340 nm for 2 min in an assay mixture containing 10 µg mitochondrial protein in 50 mmol/L potassium phosphate buffer (pH 7.5), 1 mg/mL BSA, 250 µmol/L KCN, and 6 µL of ubiquinone₁ (10 mM) in a 1-mL cuvette on a DS-11 FX + spectrophotometer (DeNovix, Wilmington, DE). In parallel, NADH oxidation was measured in the presence of complex I inhibitor rotenone (10 µmol/L) in the above assay mixture for 2 min. Subsequently, complex I activity was calculated as rotenone-sensitive activity expressed as nanomoles/minute per milligram of mitochondrial protein. Complex II activity was determined by measuring the reduction of 2,6-dichlorophenolindophenol coupled to complex II catalyzed reduction of decylubiquinone. Briefly, 10 µg mitochondrial protein in 50 mmol/L potassium phosphate buffer (pH 7.5), 1 mg/mL BSA, and 20 mmol/L succinate was incubated at 37°C for 10 min following measurement of 2,6-dichlorophenolindophenol (DCPIP) reduction in the presence of 10 µmol/L antimycin A, 10 µmol/L rotenone, 250 µmol/L KCN, 80 µmol/L DCPIP, and 60 µmol/L decylubiquinone at 600 nm for 3 min. Complex III activity was determined by measuring the reduction of cytochrome C (75 µmol/L) at 550 nm for 2 min in the reaction mixture containing 5 µg mitochondrial protein in 50

mmol/L potassium phosphate buffer (pH 7.5), 250 $\mu\text{mol/L}$ KCN, 100 $\mu\text{mol/L}$ EDTA, and 60 $\mu\text{mol/L}$ decylubiquinol. In parallel, in the same assay mixture, reduction of cytochrome C was measured in the presence of complex III inhibitor antimycin A (10 $\mu\text{mol/L}$) for 2 min at 550 nm.

Specific complex III activity was calculated as antimycin A-sensitive activity expressed as nanomoles/minute per milligram of mitochondrial protein. Extinction coefficient values for NADH (6.2 $\text{mM}^{-1} \text{cm}^{-1}$), DCPIP (19.1 $\text{mM}^{-1} \text{cm}^{-1}$), and reduced cytochrome C (18.5 mM^{-1}

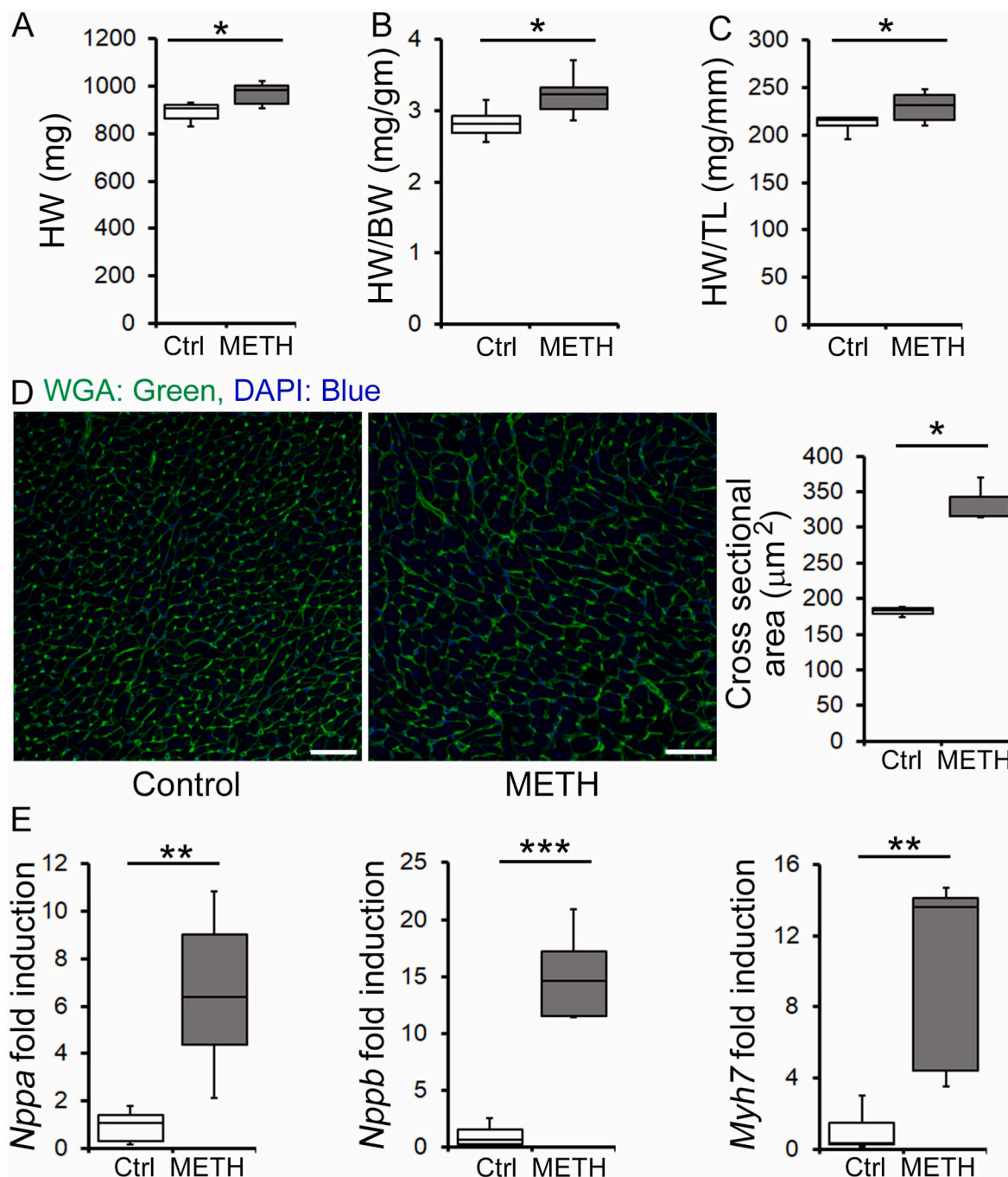


Fig. 1. METH-exposed rat hearts developed pathological cardiac hypertrophy. Box plots represent increased (A) heart weight (HW), (B) heart weight-to-body weight ratio (HW/BW), and (C) heart weight-to-tibia length ratio (HW/TL) in METH self-administered rat hearts ($n = 3$ male and 3 female rats) compared to control rat hearts ($n = 3$ male and 3 female rats) following 8-weeks of METH intake. (D) Left panel, representative immuno-fluorescence micrographs of wheat germ agglutinin (WGA, Green)-stained control and METH rat left ventricular (LV) heart sections. Nuclei were stained with DAPI (Blue). Scale bars: 50 μm . Right panel, box plots representing increased LV cardiomyocytes cross-sectional areas (μm^2) in METH self-administered rat hearts ($n = 1156$ cardiomyocytes from three individual male rat hearts) than control group rat hearts ($n = 1062$ cardiomyocytes from three individual male rat hearts). (E)–(F) Box plots depict significantly increased mRNA transcripts expression levels of natriuretic peptide A (*Nppa*), natriuretic peptide B (*Nppb*), and β -myosin heavy chain (*Myh7*) in METH self-administered rat hearts compared to control recipient rat hearts ($n = 3$ male rats/group in technical triplicates). Boxes represent interquartile ranges, lines represent medians, and whiskers represent ranges. All data sets were tested for Normality (Gaussian) distribution through Shapiro-Wilk test. Data sets that passed normality distribution were subjected to unpaired Student's t-test and data sets without normality distribution were subjected to Kruskal-Wallis test to determine statistical significance between control and METH group of rats. A P value less than 0.05 between groups was accounted as statistically significant. * $P < 0.05$, ** $P < 0.01$ and *** $P < 0.001$. Ctrl, Control; METH, Methamphetamine. (For interpretation of the references to colour in this figure legend, the reader is referred to the Web version of this article.)

cm^{-1}) were used to calculate complex I, II, and III activities, respectively [57].

2.17. Statistical analyses

All data are expressed in box plots where boxes represent inter-quartile ranges, lines represent medians, and whiskers represent ranges. All cell culture experiments were conducted in two to three independent experiments. All statistical analyses were conducted in GraphPad Prism (La Jolla, CA). All data were tested for normality distribution using Shapiro-Wilk test. Data that passed the normality assumption were analyzed using parametric tests following multiple comparisons. Unpaired student's t-test for two groups and one-way ANOVA followed by Tukey's post hoc test for data sets containing 3 or more groups were utilized to determine statistical significance. Data that failed normality assumption were subjected to nonparametric Kruskal-Wallis test. A *P* value less than 0.05 was considered statistically significant.

3. Results

3.1. METH self-administered rat hearts exhibit adverse cardiac remodeling and cardiac systolic dysfunctions

METH-associated cardiomyopathy is characterized by adverse cardiac remodeling, including cardiac hypertrophy, pathological remodeling, and attenuated cardiac functions [2,13,15,17,23]. In our current study, we determined whether rats subjected to extended access METH self-administration develop METH-induced cardiomyopathy pathological features by conducting gravimetric, histologic, genes expression analysis, and echocardiographic measurements. Notably, we found that rats which self-administered METH for 8-weeks developed increased heart wet weight mass, heart weight-to-body weight, and heart weight-to-tibia length ratios compared to control rat hearts (Fig. 1A, B and C). Cardiomyocytes cross-sectional areas analysis of LV heart sections revealed increased cross-sectional areas in METH self-administered rats compared to control rat hearts (Fig. 1D). Maladaptive cardiomyocyte hypertrophy is associated with distinct genetic signatures with activation of fetal genetic programming [58]. In fact, we found increased cardiac hypertrophy markers of fetal gene expression i.e., *Nppa*, *Nppb* and *Myh7*, indicating activation of genetic profiles of cardiac hypertrophy in METH self-administered rat hearts compared to control rat hearts (Fig. 1E).

To assess whether METH self-administration for 8-weeks causes any impairment in cardiac geometry, ventricular dimensions and systolic functions, we performed non-invasive longitudinal transthoracic M-mode echocardiography on rat hearts. Notably, rats that underwent 8-weeks long METH self-administration protocol exhibited significantly attenuated cardiac systolic functional indices, including percent fractional shortening (%FS) and percent ejection fraction (%EF) compared to control group rat hearts (Fig. 2C and F). We observed an upward trend in LV internal dimension and volume at systole (LVID; s and LV Vol; s) (Fig. 2A and D) with no change in LV internal dimension and volume at diastole (LVID; d and LV Vol; d) in METH self-administered rats compared to control group (Fig. 2B and E). There were no significant differences in the heart rate (Fig. 2G), interventricular septum thickness at systole and diastole (IVS; s and IVS; d) (Fig. 2H and I), and LV posterior wall thickness at systole and diastole (LVPW; s and LVPW; d) (Fig. 2J and K) between the groups.

Next, we examined heart histology by conducting H&E, Masson's Trichrome, and Picosirius Red (PSR) staining (Fig. 3). We observed thickening of vascular smooth muscle cells in cardiac blood vessels (Fig. 3A, indicated by star) and disarray of myofibrils in METH self-administered rat left ventricular (LV) heart sections compared to control rat LV heart sections in H&E staining (Fig. 3A, indicated by black arrow). Masson's Trichrome staining revealed increased perivascular and interstitial fibrotic areas in METH self-administered rat LV heart

sections than control rat LV heart sections (Fig. 3B and D). Similarly, we observed a substantial increase in collagen deposition as revealed in our PSR staining in METH self-administered rat LV heart sections than control rat LV heart sections (Fig. 3C and D). Activation of fibrotic signaling in the heart was characterized by increased alpha-smooth muscle actin (*Acta2*), matricellular associated protein Periostin (*Postn*), and transforming growth factor-beta isoforms (*TGFB1*, *TGFB2*, *TGFB3*) gene transcripts expression [59]. To assess whether observed augmented fibrosis in METH rat hearts was associated with activation of fibrotic gene expression, we measured mRNA transcripts expression of *Acta2*, *Postn*, *TGFB1*, *TGFB2*, and *TGFB3*. We observed increased gene expression of *Acta2*, *Postn*, *TGFB1*, and *TGFB2* in METH self-administered rat hearts compared to control hearts, corroborating activation of fibrotic genes programming (Fig. 3E and F). Overall, we found notable pathological alterations, including adverse cardiac remodeling as evidenced by increased cardiomyocytes hypertrophy and myocardial fibrosis accompanied with a decline in cardiac contractile functions post chronic METH self-administration.

3.2. METH self-administration causes altered mitochondrial ultrastructure and decline in mitochondrial respiratory chain complexes abundance

An adult human heart produces and consumes nearly 6 kg of ATP daily to accommodate the energy demand to maintain its continuous mechanical workload [60,61]. In mammalian cardiac cells, mitochondria are the major site to produce ATP to supply the required chemical energy for continuous contraction-relaxation cycles [62]. Mitochondria occupy up to about one-third the volume of a cardiomyocyte and are neatly positioned along the sarcomere [60,63]. Since we have observed a decline in cardiac contractile functional indices in METH self-administered rat hearts, we performed TEM-based ultrastructural analysis on LV heart sections. Notably, we observed an increased appearance of large, abnormal-shaped mitochondria at both intermyofibrillar and perinuclear regions in METH self-administered rat heart cardiomyocytes compared to control cardiomyocytes (Fig. 4A). We further confirmed our observations through measuring mitochondrial areas evidenced by increased average mitochondrial areas in METH self-administered rat LV heart sections compared to control rat LV heart sections (Fig. 4A).

The structural and functional organization of mitochondrial super-complexes (SCs) are formed by different stoichiometric combinations of four complexes of the electron transport chain (ETC) (complexes I, II, III, and IV) embedded in the inner mitochondrial membrane [64,65]. These enzyme complexes catalyze the transfer of reducing equivalents from high-energy substrates generated in the citric acid cycle to reduce molecular oxygen to water. Furthermore, the redox energy released in these reactions is utilized to transfer protons from the mitochondrial matrix to intermembrane space, ultimately generating a proton-motive force driving ATP synthesis at complex V [64,65]. To dissect whether altered mitochondrial ultrastructure affects mitochondrial respiratory chain SCs assembly, stability, and abundance in METH-associated cardiomyopathy hearts, we conducted blue native PAGE (BN-PAGE) on isolated mitochondria preparations allowing protein separation under native conditions and preserving protein-protein interactions, which is important for studying SCs. Intriguingly, we observed an apparent decreased level of native respiratory chain SCs, i.e., complex I, complex II, complex IV, and complex V, in METH self-administered rat heart mitochondria compared to control rat heart mitochondria (Fig. 4B). Further, antibody-mediated detection of SCs revealed significantly reduced expression of complex II, complex III, complex IV and complex V subunits in METH self-administered rat hearts compared to control rat hearts (Fig. 4C and D). Taken together, we found chronic METH self-administration induces mitochondrial ultrastructural anomalies with altered mitochondrial respiratory chain SCs assembly and expression in rat hearts.

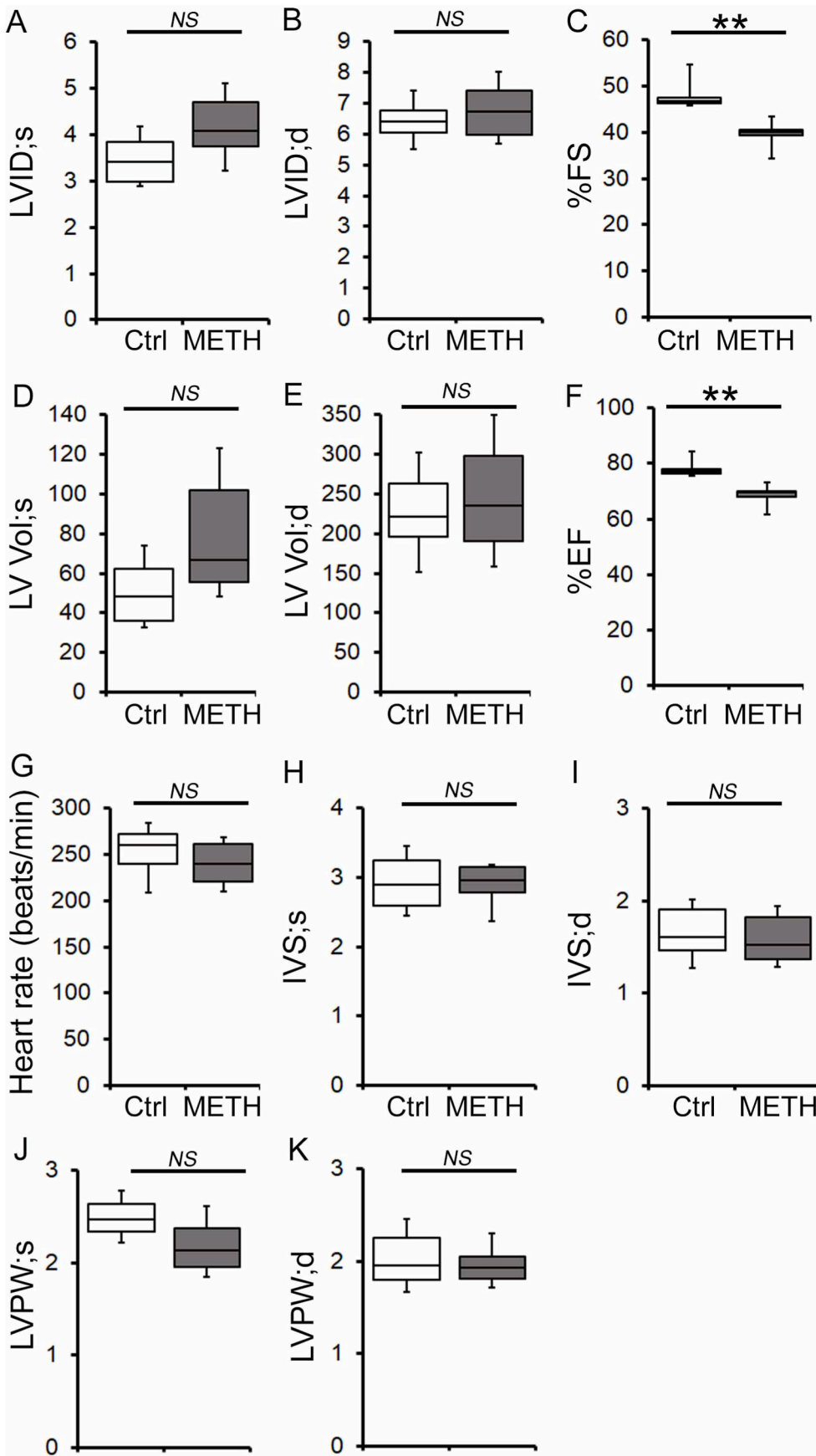
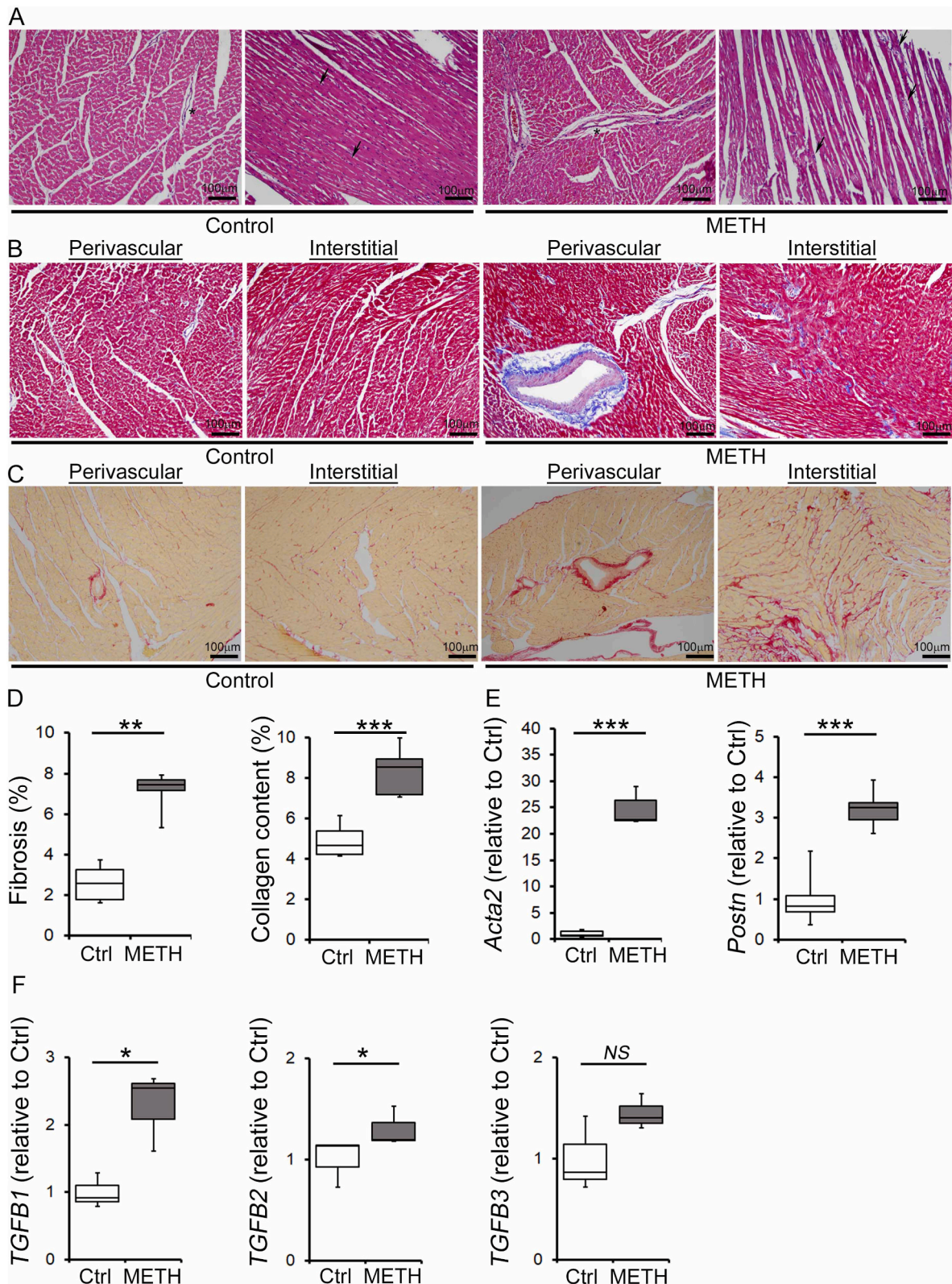


Fig. 2. Rats that self-administered METH exhibited cardiac systolic functional parameters decline. (A)–(K) Box plots represent cardiac left ventricular (LV) structural and functional indices measured by transthoracic M-mode echocardiography in control (n = 3 male and 3 female rats) and self-administered METH (n = 3 male and 3 female rats) rats post 8-weeks of METH self-administration. METH self-administration ensued in significant attenuation in cardiac systolic functional parameters including percent fractional shortening and percent ejection fraction compared to control rat hearts. (A) LV internal diameter at systole (LVID; s). (B) LV internal diameter at diastole (LVID; d). (C) Percent fractional shortening (%FS). (D) LV volume at systole (LV Vol; s). (E) LV volume at diastole (LV Vol; d). (F) Percent ejection fraction (%EF). (G) Heart rate (beats/min). (H) LV interventricular septum thickness at systole (IVS; s). (I) LV interventricular septum thickness at diastole (IVS; d). (J) LV posterior wall thickness at systole (LVPW; s). (K) LV posterior wall thickness at diastole (LVPW; d). Boxes represent interquartile ranges, lines represent medians, and whiskers represent ranges. All data were tested for Normality (Gaussian) distribution through Shapiro-Wilk test. Data sets that passed normality distribution were subjected to parametric unpaired Student's t-test and data sets without normality distribution were subjected to nonparametric Kruskal-Wallis test to determine statistical significance between control and METH group of rats. A P value less than 0.05 between groups was accounted as statistically significant. Ctrl, Control; METH, Methamphetamine.



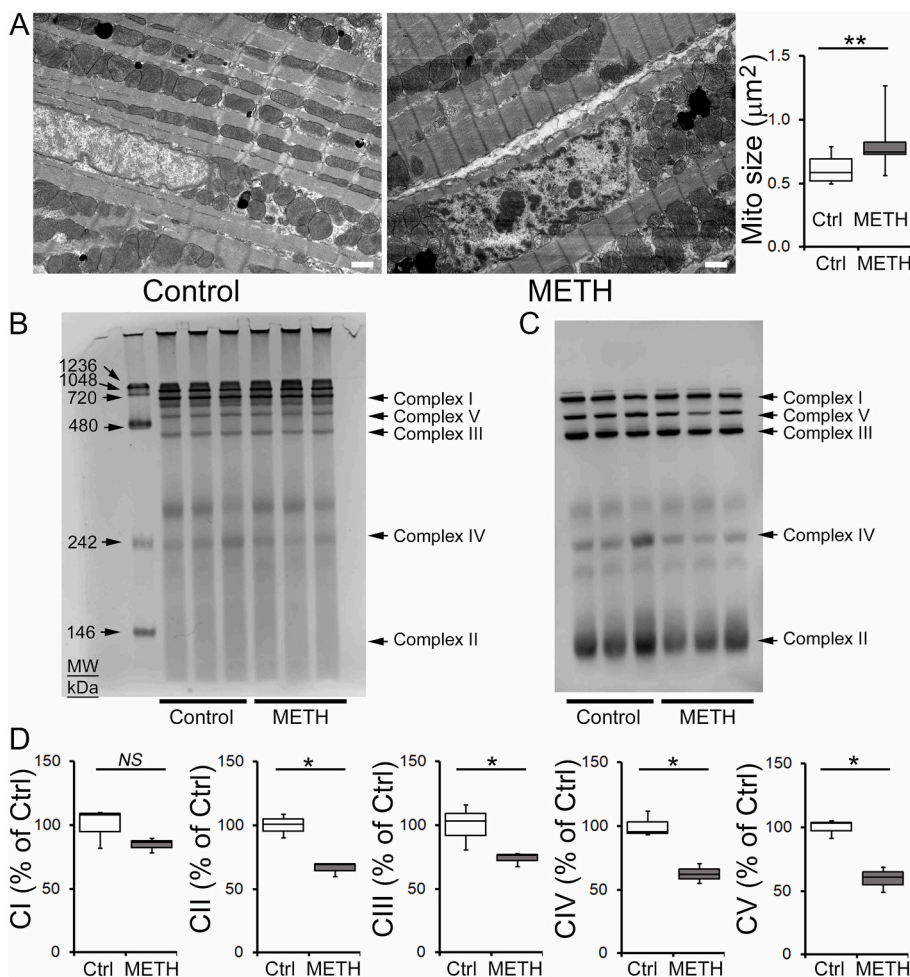
(caption on next page)

3.3. METH self-administered rat hearts exhibited decline in mitochondrial respiratory ETC complexes activity and increased PDH activity

To assess whether mitochondrial structural alterations and disruption of the respiratory ETC SCs influence overall mitochondrial function, we conducted redox-sensitive spectrophotometric assays [57]. Notably,

we observed significantly reduced specific enzymatic activity of mitochondrial respiratory ETC complex I, complex II, and complex III in METH self-administered rat heart mitochondria compared to control rat heart mitochondria (Fig. 5A, B, and C). These data extend METH self-administered rat hearts mitochondrial respiratory SCs stability alterations resulting in their functional impairments.

Fig. 3. Rats that self-administered METH exhibited altered cardiac histology and increased fibrosis. **(A)** Representative cross-sectional and longitudinal H&E-stained left ventricular (LV) heart section micrographs demonstrate thickening of vascular smooth muscle cells layer (indicated by star) and evidence of disarray of myofibrils and myofiber loss (indicated by black arrow) in METH self-administered rat hearts ($n = 2$ male and 2 female rats) compared to control rat LV heart sections ($n = 2$ male and 2 female rats). Scale bars: 100 μm . **(B)** Representative Masson's Trichrome stained LV heart section micrographs demonstrate increased perivascular and interstitial fibrotic areas (in blue) in METH self-administered rat hearts ($n = 3$ male and 3 female rats) compared control rat hearts ($n = 3$ male and 3 female rats). Scale bars: 100 μm . **(C)** Representative Picrosirius red stained heart section micrographs show exacerbated collagen deposition (in red) in perivascular and interstitial spaces in METH rat hearts ($n = 3$ male and 3 female rats) compared to control rat hearts ($n = 3$ male and 2 female rats). Scale bars: 100 μm . **(D)** Left panel, box plots represent increased percent fibrosis areas in METH rat hearts ($n = 3$ male and 3 female rats) compared to control rat hearts ($n = 3$ male and 3 female rats). Right panel, box plots represent increased percent collagen content in METH rat hearts ($n = 3$ male and 3 female rats) compared to control rat hearts ($n = 3$ male and 2 female rats). **(E)** Box plots represent significantly increased alpha-smooth muscle actin (*Acta2*) and Periostin (*Postn*) mRNA transcripts abundance in METH rat myocardium compared to control rat hearts ($n = 3$ male rats/group in technical triplicates). **(F)** Box plots represent increased transforming growth factor-beta-isoforms $\beta 1$ (*TGFB1*) and $\beta 2$ (*TGFB2*) mRNA transcripts abundance in METH rat myocardium compared to control rat hearts ($n = 3$ male rats/group in technical triplicates). Boxes represent interquartile ranges, lines represent medians, and whiskers represent ranges. All data sets were tested for Normality (Gaussian) distribution through Shapiro-Wilk test. Data sets that passed normality distribution were subjected to parametric unpaired Student's t-test, and data sets without normality distribution were subjected to a nonparametric Kruskal-Wallis test to determine statistical significance between the control and METH group of rats data. A P value less than 0.05 between groups was accounted as statistically significant. * $P < 0.05$, ** $P < 0.01$ and *** $P < 0.001$. Ctrl, Control; METH, Methamphetamine. (For interpretation of the references to colour in this figure legend, the reader is referred to the Web version of this article.)



PDH is a mitochondrion-located, multiprotein enzyme complex that connects glycolysis to tricarboxylic acid cycle (TCA) to generate energy substrates to supply to mitochondrial ETC-supported oxidative phosphorylation (OXPHOS) [66,67]. Since we observed impaired

mitochondrial ETC complexes activity, we asked whether METH affects PDH activity in cardiac mitochondria. Therefore, we measured PDH activity as a function of the rate of production of nanomoles of NADH in isolated mitochondria from METH self-administered and control rat

hearts. We observed increased PDH activity in METH self-administered rat hearts mitochondria compared to control rat hearts (Fig. 5D). Citrate synthase (CS) activity was used to normalize the mitochondrial content and purity of the isolated mitochondria [68]. We have found no significant difference in citrate synthase activity between METH self-administered and control rat hearts (Fig. 5E), indicating a similar amount of mitochondria used for the complex activity among groups. Altogether, our data suggest activation of adaptive PDH activity in response to impaired mitochondrial respiratory complex activities in METH self-administered rat heart mitochondria.

3.4. METH self-administration activates autophagy indicative decline in cellular energy homeostasis in rat hearts

Macro-autophagy or also referred as autophagy is a conserved self-eating catabolic process involved in the degradation of intracellular components including soluble proteins, aggregated, misfolded proteins, damaged organelles, macromolecular complexes, and foreign bodies

[69,70]. Accumulating research reported substantial evidence of autophagy induction under energy-deprived conditions as an adaptive mechanism of dwindling energy in cells [71,72]. We have previously reported METH treatment significantly reduces mitochondrial oxygen consumptions and bioenergetics profile in isolated cardiac mitochondria and primary neonatal rat cardiomyocytes [23]. To this point, in our current study, we extended our previous findings and observed defects in cardiomyocytes major energy source ETC SCs integrity, reduced mitochondrial complex specific activities with concomitant increased mitochondrial glucose oxidation pathway regulatory PDH complex activity in METH self-administered rat heart mitochondria. These data suggest impaired mitochondrial energy production with activation of compensatory energy production pathway in METH exposed rat hearts mitochondria. To assess the autophagy process, we conducted immunoblotting experiments to quantitate initial phagophore forming complex partner protein Beclin1, adaptor protein p62, mature autophagosomes membrane protein LC3B-II, and lysosomal enzyme Cathepsin D expression in heart lysates. Notably, we observed a

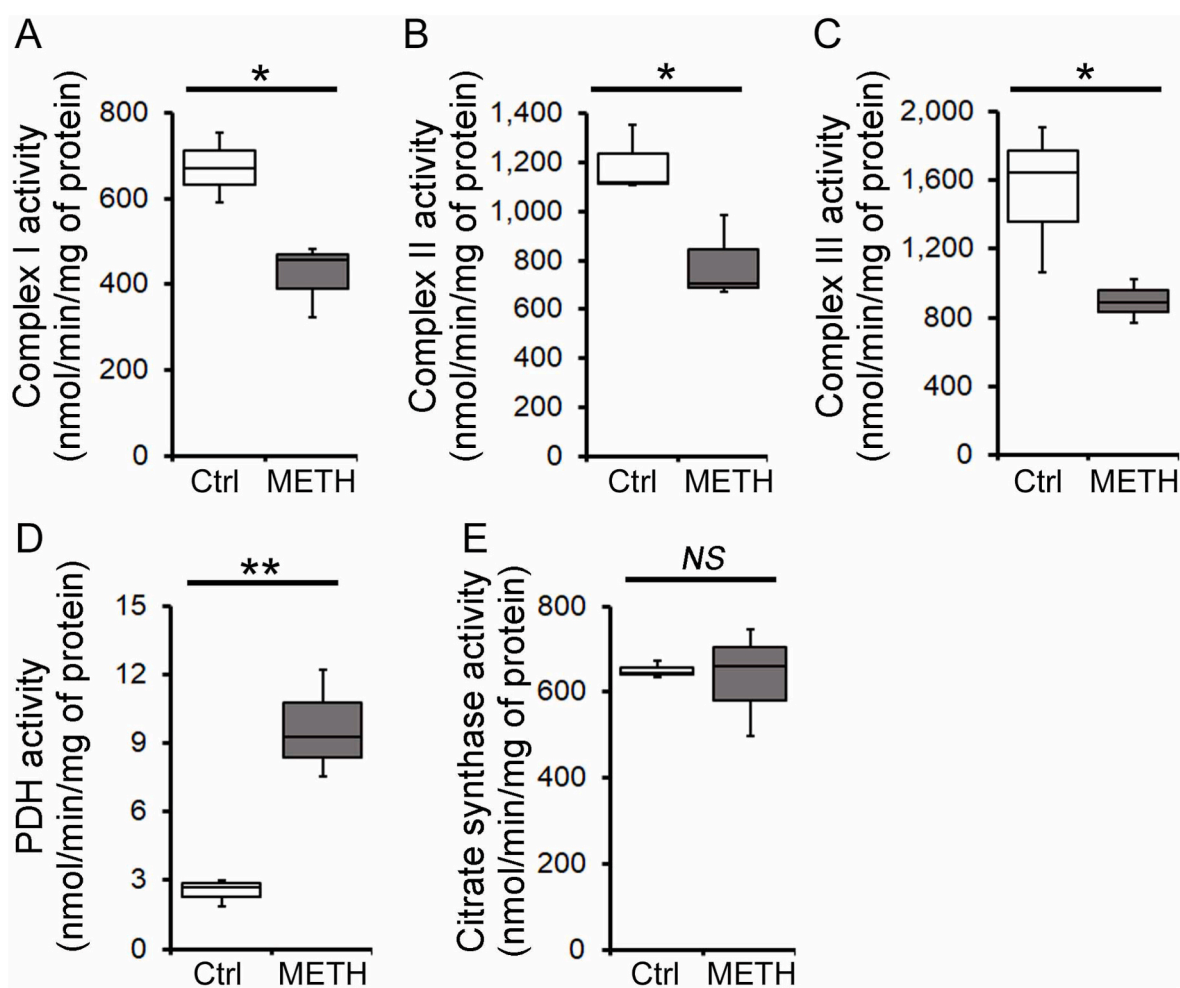


Fig. 5. METH self-administration ensues defective mitochondrial respiratory chain complexes enzymatic activities with compensatory increased PDH activity in rat heart mitochondria. Box plots represent mitochondrial respiratory chain complexes' specific enzymatic activities of (A) Complex I, (B) Complex II, and (C) Complex III. Mitochondria were isolated from rat heart ventricles and mitochondrial inner membrane located respiratory chain complexes were exposed through three freeze and thaw cycles. Respiratory chain complexes specific enzymatic activities were measured spectrophotometrically in presence of complex specific electron donating substrates and subtracting underlying non-specific activities upon respective complexes inhibitor addition. Specific complex activities were expressed as nmol per minute per mg of mitochondrial protein ($n = 3$ individual male rat heart isolated mitochondria preparations per treatment group) (D) Box plots represent spectrophotometrically measured PDH activity as a function of cardiac mitochondria capability to produce reduced nmol NADH per minute per mg of protein isolated from Control and METH self-administered rat hearts ($n = 3$ individual male rat hearts per group). (E) Box plots represent measured mitochondrial matrix enzyme citrate synthase activity in control and METH self-administered rat hearts ($n = 3$ male and 2 female individual rats per group). Enzymatic activity is expressed as nmol per minute per mg of protein. Boxes represent interquartile ranges, lines represent medians, and whiskers represent ranges. Data were subjected to nonparametric Kruskal-Wallis test to determine statistical significance between control and METH group of rats data. A P value less than 0.05 between groups was accounted as statistically significant. * $P < 0.05$ and ** $P < 0.01$. Ctrl, Control; METH, Methamphetamine.

significantly increased level of LC3B II, p62, Beclin1, and Cathepsin D in METH self-administered rat hearts compared to control rat hearts (Fig. 6A). We used GAPDH as a loading control. To answer whether METH exposure directly induces autophagy flux, we utilized primary neonatal rat ventricular cardiomyocytes (NRCs). We performed an autophagy flux assay by blocking lysosomal degradation using Bafilomycin A1 (BafA1) under vehicle and METH (100 μ M) treatment (Fig. 6B). Assessment of autophagy flux in cardiomyocytes showed that METH exposure significantly increased LC3B II compared to control NRCs (Fig. 6B). Notably, BafA1 treatment further increased LC3B II and p62 levels in METH group NRCs compared to control NRCs treated with BafA1 (Fig. 6B) indicating intact and increased autophagy flux under METH treatment. To further corroborate that increased accumulation of LC3B-II indeed due to increased synthesis of autophagosomes under METH treatment, we used class III PtdIns3k inhibitor Wortmannin to inhibit autophagosomes formation. Indeed, Wortmannin treatment reduced the accumulation of LC3B-II in cardiomyocytes compared to the METH and METH + BafA1 group (Fig. 6C). Moreover, Wortmannin treatment in METH group increases p62 levels compared to METH only treated cardiomyocytes (Fig. 6C). To further confirm the autophagy activation by METH, we genetically ablated E1-like ligase enzyme Atg7 in cardiomyocytes [73]. Atg7 siRNA treated cardiomyocytes exhibited significantly reduced LC3B-II level compared to control siRNA treated cardiomyocytes under vehicle and BafA1 treatment (Fig. 6D). Remarkably, METH failed to accumulate mature LC3B-II in Atg7 siRNA treated cardiomyocytes under vehicle and BafA1 treatment compared to control siRNA and METH treated cardiomyocytes (Fig. 6D). In addition, METH treatment further increases p62 levels in Atg7 siRNA cardiomyocytes compared to control siRNA + METH treated cardiomyocytes (Fig. 6D). Altogether, our data demonstrates that METH induces autophagy flux as evidenced through our systematic analysis using autophagosome-lysosomal fusion inhibitor (BafA1), autophagosomes formation inhibitor (Wortmannin), and Atg7 siRNA.

3.5. Mitochondria targeted antioxidant mitoTEMPO limits METH-induced autophagy in cardiomyocytes

Compromised mitochondrial respiratory chain complexes assembly, stability and activity cause increased leakage of lone pair electrons that lead to generate superoxide anion radicals (O_2^-) initiating chain reaction to generate reactive oxygen species (ROS) [74,75]. Cellular antioxidant system neutralizes superoxide and ROS to maintain redox homeostasis. Therefore, we observed the proteins levels of the principal antioxidant enzymes including superoxide dismutase, glutathione peroxidase, and catalase. Notably, we found METH self-administered rat hearts have increased protein levels of mitochondrial matrix localized manganese superoxide dismutase (MnSOD) without significant changes in predominantly cytosolic resident copper-zinc SOD (SOD1), glutathione peroxidase 1 (GPx) and catalase expression compared to control rat hearts (Fig. 7A). As we observed only changes in the MnSOD in the METH hearts, we treated the METH treated cardiomyocytes with pharmacological mitochondria targeted ROS scavenger to mitigate observed alterations in MnSOD expression and autophagy activation [76]. Remarkably, mitochondria-targeted antioxidant mitoTEMPO attenuates MnSOD expression with concomitant decrease in LC3B-II and p62 levels compared to METH only treated cardiomyocytes (Fig. 7B). Altogether, our data suggest that METH-induced mitochondrial dysfunction may activate an adaptive increase in autophagy as treatment with mitoTEMPO significantly reduced the METH-induced autophagy induction.

4. Discussion

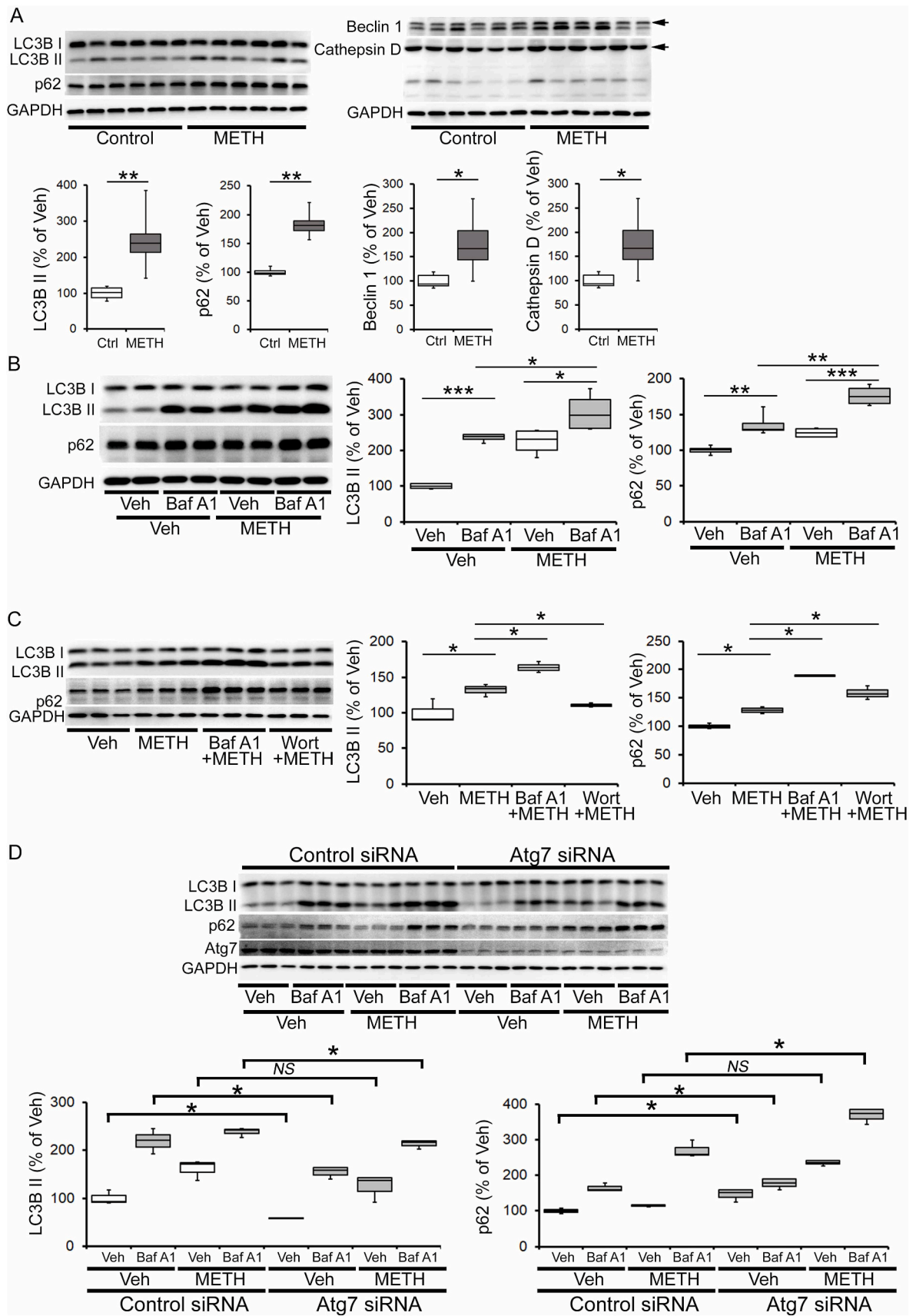
According to the recent World Drug Report (2021), illicit use of METH is highest in North America compared to the rest of the world [77]. METH-induced cardiovascular pathologies have been reported as the second leading cause of death in persons who use METH following

accidental overdose [2,8]. Along the same lines of earlier reports, a recent retrospective, large national cross-sectional studies reported a substantial increase in heart failure (HF) prevalence, HF hospitalizations, and worsening of cardiac functions in relatively young (<50 years) patients who use METH without pre-existing conditions and common comorbidities (i.e., diabetes, hypertension, coronary artery disease, and hyperlipidemia than non-METH control patients) [78,79]. METH-related HF admissions-related cost has been estimated at nearly \$390 million based on the data from a single US state [80]. Altogether, the epidemic nature of METH abuse and the socioeconomic burden posed by METH-associated cardiovascular diseases on the US public health and economy warrant coordinated effort in both biomedical research and clinical settings.

Despite the well-documented presence of cardiac pathologies and cardiomyopathy in individuals who use METH, research efforts to dissect cellular and molecular mechanisms of METH-associated cardiomyopathy remain understudied. Prevalent inadequacies in METH-cardiomyopathy research and literature include sporadic, cursory, acute studies and lack of utilization of rodent METH-addiction models closely simulating drug-taking behavior as observed in people suffering from METH addiction [27,30,81,82]. In our current study, we utilized previously reported METH extended access self-administered rat model mimicking the 'binge and crash' pattern seen in humans suffering with METH addiction to pragmatically study the mechanisms of METH-associated cardiomyopathy [35,37,38,41]. We assessed whether METH self-administered rat hearts exhibit pathological features of METH-associated cardiomyopathy and studied the molecular events associated with cardiac dysfunction.

Accumulating endomyocardial biopsy-based histologic and echocardiography studies noted increased heart mass, myocytes loss, necrotic foci, inflammatory cell infiltration, extensive interstitial, and perivascular fibrosis, altered ventricular dimensions and volume with compromised LVEF in people who use METH [9,17,19,78,83–86]. In our current study, our complementary gravimetric and histologic studies revealed increased heart weight and augmented cardiomyocytes cross-sectional areas in rat hearts subjected to 8-weeks of METH self-administration 'binge and crash' regime compared to age- and gender-matched control rats. A recent retrospective study identified abnormal brain natriuretic peptide (BNP) levels as a predictor of severe cardiac dysfunction (%LVEF <30%) in logistic regression analysis in METH HF patients [87]. Another retrospective study reported elevated BNP/pro-BNP levels corresponded to 90% documented HF in patients who use METH [79]. Fetal gene program (ANP, BNP and β -MHC) activation is a maladaptive response to HF in adult hearts and is utilized as marker of cardiac hypertrophy [88]. In our study, we observed significantly increased ANP, BNP, and β -MHC genes expression, corroborating our morphologic and histopathologic findings of cardiac hypertrophy in METH self-administered rat heart ventricles. To substantiate our findings, we conducted longitudinal transthoracic echocardiography studies. Our LV tracing-based echocardiogram analysis of LV dimensions, volume, and systolic indices revealed altered end-systolic LV internal dimension and volume with significantly attenuated LV percent ejection fraction and fractional shortening in METH self-administered rat hearts compared to control hearts.

Cardiac fibrosis is characterized by excessive deposition of extracellular matrix proteins due to maladaptive activation of a reparative program under pathogenic stressors in the heart [59,89]. Enhanced fibrosis is a common pathophysiologic companion in most cardiac pathologic conditions [59]. There are cumulative clinical case studies reporting the presence of increased fibrosis in hearts of people who use METH [15,23]. In our study, we observed hyperplasia in vascular smooth muscle cell layers, myofibers wasting, and disarray in H&E-stained LV heart sections in METH self-administered rat hearts compared to control rat hearts. Further, we observed significantly increased fibrosis area and collagen deposition in METH self-administered rat hearts compared to control rat hearts. Activated



(caption on next page)

Fig. 6. METH self-administration increases autophagy-related proteins expression and autophagic flux in cardiomyocytes. (A) Upper panel, representative Western blot images showing level of proteins involved in the autophagy process, i.e., LC3B-I, LC3B-II, p62, Beclin1 and Cathepsin D in heart whole cell lysates of control and METH self-administered rats. GAPDH was used as a loading control. Lower panel, box plots show densitometric quantification of LC3B-II, p62, Beclin1 and Cathepsin D protein levels as fold change to the control group ($n = 3$ male and 3 female rats per group). Data were subjected to nonparametric Kruskal-Wallis test to determine statistical significance. (B) Left panel, representative Western blot images showing autophagy flux assay results in vehicle and METH treated primary neonatal rat cardiomyocytes (NRCs). NRCs were treated with saline (vehicle) and METH (100 μ M, dissolved in saline) for 24 h. Bafilomycin A1 (50 nmol/L) was added for 3 h to block lysosomal degradation. METH treatment significantly increased autophagy flux in cardiomyocytes as evident in increased LC3B-II and p62 protein levels in METH + BafA1 treated NRCs compared to Saline + BafA1 and METH only treated NRCs. GAPDH was used as a loading control. (C) Representative western blot and densitometric quantification demonstrate METH (100 μ M for 24 h) significantly increased autophagy proteins LC3B-II and p62 compared to Vehicle treated NRCs which further increased post BafA1 (50 nmol/L for 3 h) treatment. However, METH treated (100 μ M for 24 h) NRCs failed to increase mature autophagosome protein LC3B-II level in the presence of PI3K inhibitor Wortmannin (1 μ M for 3 h) compared to METH-only treated NRCs. Interestingly, Wortmannin-treated NRCs exhibit increased accumulation of p62 compared to METH-only treated NRCs. GAPDH was used as a loading control. (D) Representative western blot and densitometric quantification demonstrate both Vehicle and METH (100 μ M for 24 h) treated NRCs failed to increase mature autophagosome protein LC3B-II level following autophagy-related protein Atg7 siRNA (50 nM) mediated knockdown under baseline and BafA1 (50 nmol/L for 3 h) treatment compared to control siRNA treated NRCs. Notably, Atg7 knockdown further accumulated p62 levels in METH and METH + BafA1 treated NRCs. GAPDH was used as a loading control. Boxes represent interquartile ranges, lines represent medians, and whiskers represent ranges. Data were subjected to One-Way ANOVA followed by Tukey's multiple comparisons test to determine statistical significance among the groups. A P value less than 0.05 between groups was accounted as statistically significant. * $P < 0.05$, ** $P < 0.01$ and *** $P < 0.001$. Ctrl, Control; Veh, Vehicle; METH, Methamphetamine; BafA1, Bafilomycin A1; Wort, Wortmannin.

cardiac fibroblasts express genes associated with the contractile element (i.e., α SM actin) and matricellular-associated proteins (e.g., periostin) [59]. To this point, we found significantly increased *Acta2*, *Postn*, *TGFB1*, and *TGFB2* genes expression in METH self-administered rat hearts, corroborating activation of fibrotic signaling following METH exposure. Altogether, our studies revealed METH self-administration for 8-weeks resulted in salient METH-induced cardiomyopathy features constituting increased cardiac mass, cardiomyocytes hypertrophy, altered histopathology with increased interstitial and perivascular fibrosis ensued in compromised cardiac systolic functional indices.

Mitochondrial oxidative phosphorylation (OXPHOS) at electron transport chain (ETC) respiratory SCs is the central hub of energy production in the form of ATP in cardiomyocytes [64]. Defects in mitochondrial metabolism and energy production contributed to HF development under diverse pathological conditions, i.e., ischemia-reperfusion injury, pressure overload, lipid toxicity, and cardiotoxic drugs [40,90–92]. Previous studies reported METH exposure induces mitochondrial dysfunctions in both cardiovascular and neurological systems [28,93–95]. We have previously reported reduced mitochondrial respiration in mice heart mitochondria exposed for 4-weeks of intraperitoneal dose-escalated 'binge and crash' METH paradigm [23]. In our study, to dissect the underlying causes of reduced cardiac functions in METH self-administered rat hearts, we conducted complementary ultrastructural, biochemical, and redox-sensitive spectrophotometric assays in ultra-thin heart sections and isolated cardiac mitochondria. In our ultrastructural analysis, we observed abnormal, large mitochondria accumulation in METH self-administered rat LV heart sections as reflected in increased mitochondrial areas compared to control rat LV hearts at TEM level. Our further studies revealed a decline in mitochondrial respiratory ETC SCs assembly and SCs subunits expression at native gel electrophoresis in METH self-administered rat hearts mitochondria compared to control rat hearts. Redox assays utilizing complex specific substrates and inhibitors revealed significantly attenuated specific activity of mitochondrial respiratory ETC complex I, complex II, and complex III in METH self-administered rat hearts.

Under physiologic conditions, fatty acid oxidation (FAO) predominates to supply reducing equivalents for mitochondrial OXPHOS to generate 60–70% ATP in the mammalian heart [60–62]. The remaining is primarily generated by glucose oxidation with a lesser extent of amino acids and ketone bodies oxidation [60,61]. However, pathological cardiac hypertrophy is associated with a shift in myocardial fuel metabolism preference from FAO to increased reliance on glucose [96,97]. Multi-enzyme complex PDH at mitochondria plays a regulatory role in glucose oxidation through decarboxylation of pyruvate to acetyl-coA that links cytosolic glycolysis to mitochondrial ETC substrate producing TCA cycle [66,67]. To this point, PDH multi-enzyme complex expression and activity has been reported to be increased in human

systolic HF patients [98]. In our current study, we have observed increased PDH activity measured as the production rate of nanomoles of NADH in mitochondria from METH self-administered rat hearts compared to control hearts. Hence, our data suggest METH self-administration causes impaired mitochondrial ultrastructure, compromised ETC SCs assembly, and defects in mitochondrial energy generating OXPHOS complexes activity accompanied by a compensatory increase in PDH activity post-8-weeks of METH exposure.

Cellular autophagy activity coordinates with energy reserve and mitochondria-derived ROS [71,72,99]. Under these conditions, autophagy activity has been shown to be increased, whereas overexpression of antioxidant enzymes has been shown to normalize ROS-induced autophagy [100,101]. Remarkably, we found an increased accumulation of autophagy-related proteins involved in phagophore initiation complex partner protein Beclin1, mature autophagosome marker protein LC3B-II, adaptor protein p62, and lysosomal enzyme cathepsin D in METH self-administered rat hearts than control rat hearts. The accumulation of LC3B-II can be either due to increased synthesis of autophagosomes or blockage of downstream lysosomal degradation pathways. Therefore, we conducted an autophagy flux assay in the presence of lysosomal acidification inhibitor BafA1, which inhibits autophagosomes and lysosome fusion in primary cardiomyocytes. Notably, we found a further increase in LC3B-II levels in METH-exposed cardiomyocytes treated with BafA1 compared to control and BafA1-treated cardiomyocytes. To further test whether METH treatment induced increased LC3B-II levels is not because of downstream blockage of lysosomal degradation of autophagosomes, we treated cardiomyocytes with PI3K inhibitor Wortmannin which inhibits autophagosome formation in the presence of METH [102]. Notably, METH failed to accumulate LC3B-II levels to a level quantitated in METH only and METH with BafA1-treated cardiomyocytes. To corroborate these findings, we further genetically ablated Atg7, an E1-like ligase enzyme catalyzing lipidation of LC3B-I to form mature LC3B-II, to deplete autophagosomes in cardiomyocytes. Notably, we found that Atg7 siRNA knockdown significantly attenuated LC3B-II accumulation compared to control siRNA-treated cardiomyocytes under METH treatment. Under both Wortmannin treatment and Atg7 siRNA knockdown, we observed METH induces further accumulation of p62 in cardiomyocytes indicating intact METH-induced activation of autophagosome synthesis is required for cytosolic adaptor protein p62 clearance. Altogether, our complementary experimental results indicate METH treatment induces increased autophagosomes synthesis as evidenced with increased LC3B-II levels in autophagy flux assay, i.e., BafA1 and decreased LC3B-II levels in autophagosomes synthesis inhibition assays, i.e., Wortmannin, Atg7 siRNA, in cardiomyocytes. Mitochondrial superoxide ($O_2^{\cdot -}$) has been shown to be a major ROS-activating autophagy. Interestingly, Chen et al. reported overexpression of mitochondria matrix localized Mn-SOD attenuates superoxide-induced autophagy

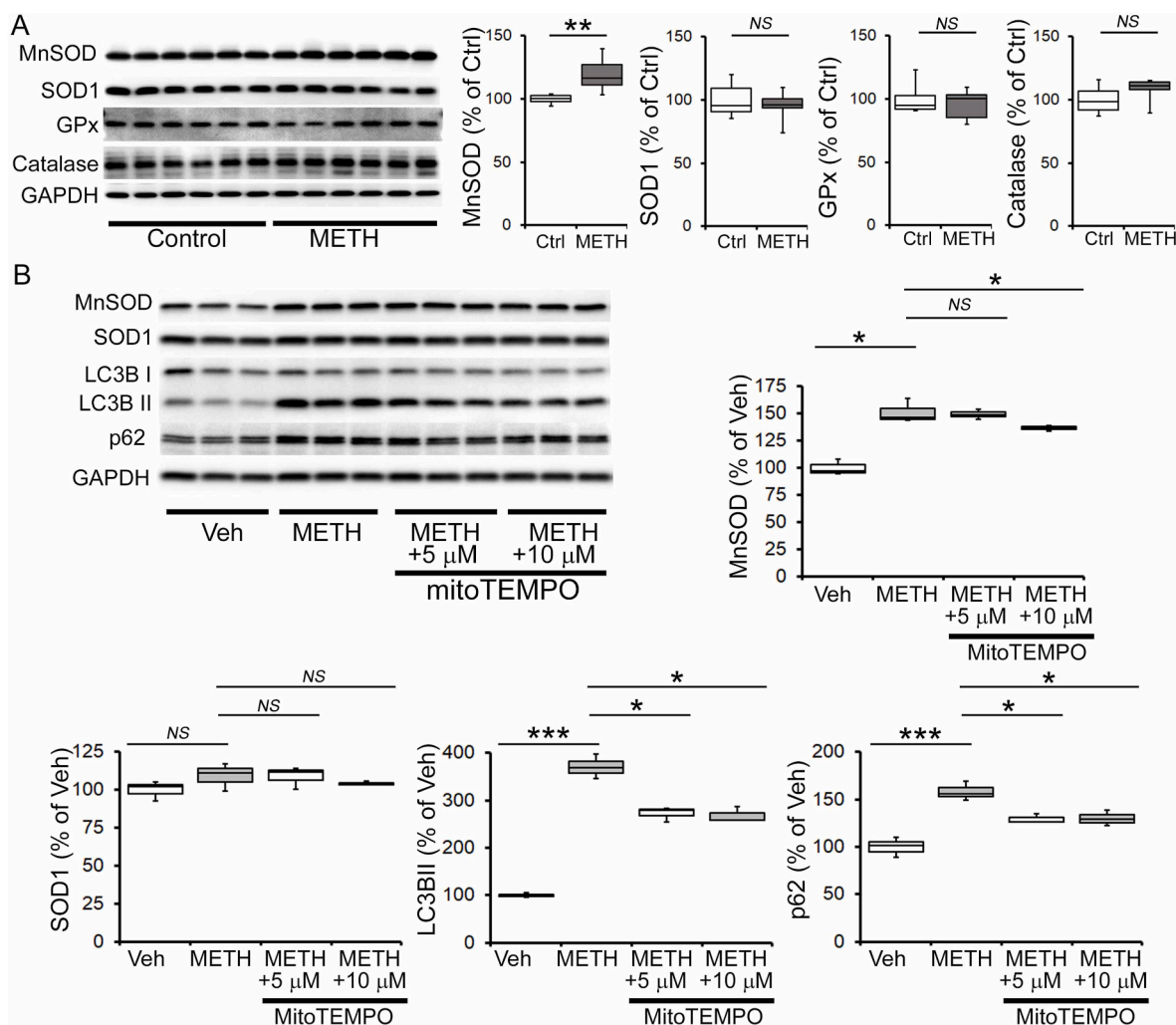


Fig. 7. Mitochondria targeted antioxidant mitoTEMPO attenuates METH-induced autophagy in cardiomyocytes. (A) Left panel, representative Western blot membrane images demonstrate cellular antioxidant proteins, i.e., MnSOD, SOD1, GPx, and Catalase, in heart whole cell lysates of control and METH self-administered rats. GAPDH was used as the loading control. Right panel, box plots show densitometric quantifications of MnSOD, SOD1, GPx, and Catalase relative expressions as percent change to Control rat hearts. $n = 3$ male and 3 female rats per group. Data were subjected to nonparametric Kruskal-Wallis test to determine statistical significance. (B) Representative Western blot images demonstrating effects of vehicle, METH, and mitoTEMPO treatment on cellular antioxidant proteins, i.e., MnSOD, SOD1 and autophagy proteins LC3B-II, and p62 in primary neonatal rat cardiomyocytes (NRCs). NRCs were treated with saline (vehicle), METH (100 μ M, dissolved in saline), and METH 100 μ M in presence of 5 μ M and 10 μ M mitoTEMPO, respectively, for 24 h. MitoTEMPO (5 μ M and 10 μ M) were added to the culture medium to quench mitochondria-derived reactive oxygen species (ROS) under METH treatment. METH treatment significantly increased mitochondria localized MnSOD expression accompanied by increased accumulation of autophagy proteins LC3B-II and p62 in NRCs compared to Vehicle-treated NRCs. Notably, mitoTEMPO (10 μ M) treatment significantly attenuates MnSOD with a concomitant reduction in autophagy proteins LC3B-II and p62 levels compared to METH-only treated NRCs. GAPDH was used as the loading control. Boxes represent interquartile ranges, lines represent medians, and whiskers represent ranges. Data were subjected to One-Way ANOVA followed by Tukey's multiple comparisons test to determine statistical significance among the groups. A P value less than 0.05 between groups was accounted as statistically significant. * $P < 0.05$, ** $P < 0.01$ and *** $P < 0.001$. Ctrl, Control; Veh, Vehicle; METH, Methamphetamine.

[101]. In our current study, we have observed increased expression of mitochondrial matrix resident superoxide dismutase enzyme MnSOD expression with no change in cytosol resident antioxidant enzymes SOD1, glutathione peroxidase, and catalase in METH self-administered rat hearts compared to control rat hearts. Therefore, we treated cardiomyocytes with mitochondria-targeted superoxide scavenger mitoTEMPO [103]. Remarkably, we observed co-treatment with mitoTEMPO significantly reduced MnSOD expression with reduced expression of autophagy regulatory proteins LC3B-II and p62 in the presence of METH compared to the cardiomyocytes treated with METH alone. These results inform potential therapeutic benefits of mitochondria-targeted ROS scavengers to limit METH-induced cardiotoxicity.

Overall, herein, we report a novel METH self-administration-associated cardiomyopathy model in rats characterized by salient histopathologic changes and cardiac dysfunctions. This 'binge and crash'

rat model pragmatically can be used in preclinical research to study molecular mechanisms of METH cardiotoxicity and test novel therapeutics. Our molecular, biochemical, and redox assays revealed chronic METH intake ensues in large, abnormal shaped mitochondria, causing a decline in mitochondrial OXPHOS SCs integrity at native state corresponding with attenuated OXPHOS complexes expression and activity with increased compensatory PDH activity suggesting altered myocardial metabolic phenotypes and plausible gene reprogramming. We also observed an increase in autophagy by METH treatment which was reduced by treatment with mitoTEMPO, indicating mitochondrial involvement in the activation of autophagy. Therefore, future studies should be aimed at conducting unbiased metabolomics and transcriptomic analysis to identify novel molecular targets in METH-induced cardiotoxicity. Furthermore, our future studies will aim to employ both pharmacological and genetic approaches to assess the therapeutic

efficacy of activating cellular mitochondria-targeted antioxidant system activation against METH-induced cardiotoxicity utilizing our reported rodent METH-cardiomyopathy models.

Author contributions

C.S.A., and M.S.B. conceptualized the study; C.S.A., N.S.R., R.A., and M.S.B. designed the experiments; C.S.A., N.S.R., R.A., S.N., and G.K.K. performed all experiments and participated in analyses; N.H., K.S.M., and N.E.G. involved in self-administration of METH in rats; N.S.R. performed primary cardiomyocytes isolation; B.H. and J.K. performed electron microscopic experiments; M.A.N.B. performed statistical analysis; J.T., A.W.O. and C.G.K. contributed to analytic tools and contributed to reagents; C.S.A. and M.S.B. wrote the manuscript, and all of the authors have read, edited, and approved the paper.

Sources of funding

This work was supported by the National Institutes of Health grants: R01HL145753, R01HL145753-01S1, R01HL145753-03S1, and R01HL152723; and LSUHSC-S CCDS Finish Line Award, COVID-19 Research Award, and Louisiana Addiction Research Center Research Award to MSB; P20GM121307 and R01 HL149264 to C.G.K.; NIH R01 HL098435, HL133497, and HL141155 to A.W.O.; NIH R01 NS120676 to K.S.M.; LSUHSC-S Malcolm Feist fellowship from the Center for Cardiovascular diseases and Sciences, and AHA Postdoctoral Fellowship to C.S.A. (20POST35210789); LSUHSC-S Malcolm Feist predoctoral fellowship from the Center for Cardiovascular diseases and Sciences to N.S.R. and LSUHSC-S Malcolm Feist postdoctoral fellowship from the Center for Cardiovascular diseases and Sciences to R.A.; T32HL1550 predoctoral fellowship supports N.H.

Declaration of competing interest

The authors declare that they have no known competing financial interests or personal relationships that could have appeared to influence the work reported in this paper.

Acknowledgments

We would like to thank the COBRE research core for technical support.

References

- [1] B. Cechova, R. Slamberova, Methamphetamine, neurotransmitters and neurodevelopment, *Physiol. Res.* 70 (S3) (2021) S301–S315.
- [2] C.G. Kevil, et al., Methamphetamine use and cardiovascular disease, *Arterioscler. Thromb. Vasc. Biol.* 39 (9) (2019) 1739–1746.
- [3] C.C. Cruickshank, K.R. Dyer, A review of the clinical pharmacology of methamphetamine, *Addiction* 104 (7) (2009) 1085–1099.
- [4] D.M. Stoneberg, R.K. Shukla, M.B. Magness, Global methamphetamine trends: an evolving problem, *Int. Crim. Justice Rev.* 28 (2) (2018) 136–161.
- [5] B. Han, et al., Methamphetamine use, methamphetamine use disorder, and associated overdose deaths among US adults, *JAMA Psychiatr.* 78 (12) (2021) 1329–1342.
- [6] C.M. Jones, et al., Methamphetamine use in the United States: epidemiological update and implications for prevention, treatment, and harm reduction, *Ann. N. Y. Acad. Sci.* 1508 (1) (2022) 3–22.
- [7] S. Darke, J. Duflou, S. Kaye, Prevalence and nature of cardiovascular disease in methamphetamine-related death: a national study, *Drug Alcohol Depend.* 179 (2017) 174–179.
- [8] P.K.V. Reddy, et al., Clinical characteristics and management of methamphetamine-associated cardiomyopathy: state-of-the-art review, *J. Am. Heart Assoc.* 9 (11) (2020), e016704.
- [9] R. Hong, E. Matsuyama, K. Nur, Cardiomyopathy associated with the smoking of crystal methamphetamine, *JAMA* 265 (9) (1991) 1152–1154.
- [10] J.P. Chen, Methamphetamine-associated acute myocardial infarction and cardiogenic shock with normal coronary arteries: refractory global coronary microvascular spasm, *J. Invasive Cardiol.* 19 (4) (2007). E89-92.
- [11] S.B. Karch, B.G. Stephens, C.H. Ho, Methamphetamine-related deaths in San Francisco: demographic, pathologic, and toxicologic profiles, *J. Forensic Sci.* 44 (2) (1999) 359–368.
- [12] P.H. Schaiberger, et al., Pulmonary hypertension associated with long-term inhalation of "crank" methamphetamine, *Chest* 104 (2) (1993) 614–616.
- [13] S.X. Zhao, et al., Clinical characteristics and outcome of methamphetamine-associated pulmonary arterial hypertension and dilated cardiomyopathy, *JACC Heart Fail* 6 (3) (2018) 209–218.
- [14] P. Dominic, et al., Stimulant drugs of abuse and cardiac arrhythmias, *Circ Arrhythm Electrophysiol* 15 (1) (2022), e010273.
- [15] S. Schurer, et al., Clinical characteristics, histopathological features, and clinical outcome of methamphetamine-associated cardiomyopathy, *JACC Heart Fail* 5 (6) (2017) 435–445.
- [16] T.K.M. Wang, et al., Poor outcomes in methamphetamine-associated cardiomyopathy—a growing health issue in New Zealand, *N. Z. Med. J.* 132 (1502) (2019) 55–66.
- [17] P.K. Reddy, et al., Characteristics of methamphetamine-associated cardiomyopathy and the impact of methamphetamine use on cardiac dysfunction, *Am. J. Cardiol.* 154 (2021) 86–91.
- [18] L. Curran, et al., Clinical correlates and outcomes of methamphetamine-associated cardiovascular diseases in hospitalized patients in California, *J. Am. Heart Assoc.* (2022), e023663.
- [19] R. Sadeghi, et al., Report of methamphetamine use and cardiomyopathy in three patients, *Daru* 20 (1) (2012) 20.
- [20] D.M. Schwab, H.A. Katus, P.W. Raake, [Cardiomyopathy in a 22-year-old man with a long history of methamphetamine abuse], *Internist* 60 (3) (2019) 304–308.
- [21] V. Batra, et al., Early onset cardiovascular disease related to methamphetamine use is most striking in individuals under 30: a retrospective chart review, *Addict Behav Rep* 15 (2022), 100435.
- [22] M.L. Scott, K.S. Murnane, A.W. Orr, Young at heart? Drugs of abuse cause early-onset cardiovascular disease in the young, *Heart* 107 (8) (2021) 604–606.
- [23] C.S. Abdullah, et al., Methamphetamine induces cardiomyopathy by Sigmar1 inhibition-dependent impairment of mitochondrial dynamics and function, *Commun Biol* 3 (1) (2020) 682.
- [24] M. Kaiho, I. Ishiyama, Morphological study of acute myocardial lesions experimentally induced by methamphetamine, *Nihon Hoigaku Zasshi* 43 (6) (1989) 460–468.
- [25] S.Y. He, et al., Cardiac muscle lesions associated with chronic administration of methamphetamine in rats, *Am. J. Forensic Med. Pathol* 17 (2) (1996) 155–162.
- [26] A. Matsuo, K. Ikematsu, I. Nakasono, C-fos, fos-B, c-jun and dusp-1 expression in the mouse heart after single and repeated methamphetamine administration, *Leg. Med.* 11 (6) (2009) 285–290.
- [27] S. Turdi, et al., Acute methamphetamine exposure inhibits cardiac contractile function, *Toxicol. Lett.* 189 (2) (2009) 152–158.
- [28] K.C. Lord, et al., Oxidative stress contributes to methamphetamine-induced left ventricular dysfunction, *Cardiovasc. Res.* 87 (1) (2010) 111–118.
- [29] M.C. Marcinko, et al., Sex influences susceptibility to methamphetamine cardiomyopathy in mice, *Phys. Rep.* 7 (6) (2019), e14036.
- [30] K. Sugimoto, et al., Methamphetamine directly accelerates beating rate in cardiomyocytes by increasing Ca²⁺ entry via L-type Ca²⁺ channel, *Biochem. Biophys. Res. Commun.* 390 (4) (2009) 1214–1220.
- [31] A.K. Molh, et al., Histopathological studies of cardiac lesions after an acute high dose administration of methamphetamine, *Malays. J. Med. Sci.* 15 (1) (2008) 23–30.
- [32] S.J. Semple, T.L. Patterson, I. Grant, Motivations associated with methamphetamine use among HIV+ men who have sex with men, *J. Subst. Abuse Treat.* 22 (3) (2002) 149–156.
- [33] A.K. Cho, W.P. Melega, Patterns of methamphetamine abuse and their consequences, *J. Addict. Dis.* 21 (1) (2002) 21–34.
- [34] S.L. Simon, et al., A comparison of patterns of methamphetamine and cocaine use, *J. Addict. Dis.* 21 (1) (2002) 35–44.
- [35] E.M. Cornett, N.E. Goeders, 96-hour methamphetamine self-administration in male and female rats: a novel model of human methamphetamine addiction, *Pharmacol. Biochem. Behav.* 111 (2013) 51–57.
- [36] V. Batra, et al., A general method for evaluating deep brain stimulation effects on intravenous methamphetamine self-administration, *JoVE* (107) (2016), e53266.
- [37] A.L. Spence, G.F. Guerin, N.E. Goeders, The differential effects of alprazolam and oxazepam on methamphetamine self-administration in rats, *Drug Alcohol Depend.* 166 (2016) 209–217.
- [38] C.M. Keller, et al., Effects of a methamphetamine vaccine, IXT-v100, on methamphetamine-related behaviors, *Psychopharmacology (Berl)* 237 (3) (2020) 655–667.
- [39] C.M. Keller, et al., Combinations of oxazepam and metyrapone attenuate cocaine and methamphetamine cue reactivity, *Drug Alcohol Depend.* 133 (2) (2013) 405–412.
- [40] C.S. Abdullah, et al., Doxorubicin-induced cardiomyopathy associated with inhibition of autophagic degradation process and defects in mitochondrial respiration, *Sci. Rep.* 9 (1) (2019) 2002.
- [41] A.L. Spence, G.F. Guerin, N.E. Goeders, Differential modulation of the discriminative stimulus effects of methamphetamine and cocaine by alprazolam and oxazepam in male and female rats, *Neuropharmacology* 102 (2016) 146–157.
- [42] C.S. Abdullah, et al., Cardiac dysfunction in the Sigma 1 receptor knockout mouse associated with impaired mitochondrial dynamics and bioenergetics, *J. Am. Heart Assoc.* 7 (20) (2018), e009775.
- [43] S. Alam, et al., Dysfunctional mitochondrial dynamic and oxidative phosphorylation precedes cardiac dysfunction in R120G-alphaB-crystallin-

- induced desmin-related cardiomyopathy, *J. Am. Heart Assoc.* 9 (23) (2020), e017195.
- [44] S. Alam, et al., Aberrant mitochondrial fission is maladaptive in desmin mutation-induced cardiac proteotoxicity, *J. Am. Heart Assoc.* 7 (14) (2018).
- [45] C.S. Abdullah, et al., The molecular role of Sigmar1 in regulating mitochondrial function through mitochondrial localization in cardiomyocytes, *Mitochondrion* 62 (2022) 159–175.
- [46] S. Alam, et al., Sigmar1 regulates endoplasmic reticulum stress-induced C/EBP-homologous protein expression in cardiomyocytes, *Biosci. Rep.* 37 (4) (2017).
- [47] R. Aishwarya, et al., Pleiotropic effects of mdivi-1 in altering mitochondrial dynamics, respiration, and autophagy in cardiomyocytes, *Redox Biol.* 36 (2020), 101660.
- [48] C.S. Abdullah, et al., Chemical architecture of block copolymers differentially abrogate cardiotoxicity and maintain the anticancer efficacy of doxorubicin, *Mol. Pharm.* 17 (12) (2020) 4676–4690.
- [49] L. Wickert, et al., Quantitative monitoring of the mRNA expression pattern of the TGF-beta-isoforms (beta 1, beta 2, beta 3) during transdifferentiation of hepatic stellate cells using a newly developed real-time SYBR Green PCR, *Biochem. Biophys. Res. Commun.* 295 (2) (2002) 330–335.
- [50] D. Seol, et al., Selection of reference genes for normalization of quantitative real-time PCR in organ culture of the rat and rabbit intervertebral disc, *BMC Res. Notes* 4 (1) (2011) 162.
- [51] Y. Zhang, Y. Si, N. Ma, Meis1 promotes poly (rC)-binding protein 2 expression and inhibits angiotensin II-induced cardiomyocyte hypertrophy, *IUBMB Life* 68 (1) (2016) 13–22.
- [52] J. Guan, et al., Elevated expression of periostin in diabetic cardiomyopathy and the effect of valsartan, *BMC Cardiovasc. Disord.* 15 (1) (2015) 90.
- [53] R.G. Ruddell, et al., Ferritin functions as a proinflammatory cytokine via iron-independent protein kinase C zeta/nuclear factor kappaB-regulated signaling in rat hepatic stellate cells, *Hepatology* 49 (3) (2009) 887–900.
- [54] P. Jha, X. Wang, J. Auwerx, Analysis of mitochondrial respiratory chain supercomplexes using blue native polyacrylamide gel electrophoresis (BN-PAGE), *Curr. Protoc. Mol. Biol.* 6 (1) (2016) 1–14.
- [55] L.J. Yan, M.J. Forster, Resolving mitochondrial protein complexes using nongradient blue native polyacrylamide gel electrophoresis, *Anal. Biochem.* 389 (2) (2009) 143–149.
- [56] X. Luo, et al., Non-gradient blue native polyacrylamide gel electrophoresis, *Curr. Protoc. Protein Sci.* 87 (2017) 19 29 1–19 29 12.
- [57] M. Spinazzi, et al., Assessment of mitochondrial respiratory chain enzymatic activities on tissues and cultured cells, *Nat. Protoc.* 7 (6) (2012) 1235–1246.
- [58] B.J. Maron, Hypertrophic cardiomyopathy: a systematic review, *JAMA* 287 (10) (2002) 1308–1320.
- [59] N.G. Frangogiannis, Cardiac fibrosis: cell biological mechanisms, molecular pathways and therapeutic opportunities, *Mol. Aspect. Med.* 65 (2019) 70–99.
- [60] J. Ritterhoff, R. Tian, Metabolism in cardiomyopathy: every substrate matters, *Cardiovasc. Res.* 113 (4) (2017) 411–421.
- [61] T. Doenst, T.D. Nguyen, E.D. Abel, Cardiac metabolism in heart failure: implications beyond ATP production, *Circ. Res.* 113 (6) (2013) 709–724.
- [62] J.S. Ingwall, Energy metabolism in heart failure and remodelling, *Cardiovasc. Res.* 81 (3) (2009) 412–419.
- [63] K. Williams, P.C.N. Ovalle, *Netter's Essential Histology*, first ed., Elsevier, Philadelphia, 2008.
- [64] W. Kuhlbrandt, Structure and function of mitochondrial membrane protein complexes, *BMC Biol.* 13 (2015) 89.
- [65] N.J. Caruana, D.A. Stroud, The road to the structure of the mitochondrial respiratory chain supercomplex, *Biochem. Soc. Trans.* 48 (2) (2020) 621–629.
- [66] J. Skerlova, et al., Structure of the native pyruvate dehydrogenase complex reveals the mechanism of substrate insertion, *Nat. Commun.* 12 (1) (2021) 5277.
- [67] M.S. Patel, et al., The pyruvate dehydrogenase complexes: structure-based function and regulation, *J. Biol. Chem.* 289 (24) (2014) 16615–16623.
- [68] S. Larsen, et al., Biomarkers of mitochondrial content in skeletal muscle of healthy young human subjects, *J. Physiol.* 590 (14) (2012) 3349–3360.
- [69] Y. Lei, D.J. Klionsky, The emerging roles of autophagy in human diseases, *Biomedicine* 9 (11) (2021).
- [70] Z. Yang, D.J. Klionsky, An overview of the molecular mechanism of autophagy, *Curr. Top. Microbiol. Immunol.* 335 (2009) 1–32.
- [71] P.W. Lin, M.L. Chu, H.S. Liu, Autophagy and metabolism, *Kaohsiung J. Med. Sci.* 37 (1) (2021) 12–19.
- [72] K.H. Kim, M.S. Lee, Autophagy—a key player in cellular and body metabolism, *Nat. Rev. Endocrinol.* 10 (6) (2014) 322–337.
- [73] J.J. Collier, et al., Emerging roles of ATG7 in human health and disease, *EMBO Mol. Med.* 13 (12) (2021), e14824.
- [74] D. Bou-Teen, et al., Mitochondrial ROS and mitochondria-targeted antioxidants in the aged heart, *Free Radic. Biol. Med.* 167 (2021) 109–124.
- [75] W. Wang, P.M. Kang, Oxidative stress and antioxidant treatments in cardiovascular diseases, *Antioxidants* 9 (12) (2020).
- [76] K. Du, A. Farhood, H. Jaeschke, Mitochondria-targeted antioxidant Mito-Tempo protects against acetaminophen hepatotoxicity, *Arch. Toxicol.* 91 (2) (2017) 761–773.
- [77] A. Latif, et al., Is methamphetamine-linked cardiomyopathy an emerging epidemic for new generation? *Curr. Probl. Cardiol.* (2021), 101042.
- [78] S.D. Dickson, et al., Methamphetamine-associated heart failure hospitalizations across the United States: geographic and social disparities, *J. Am. Heart Assoc.* 10 (16) (2021), e018370.
- [79] I.C. Thomas, et al., Clinical characteristics and outcomes of patients with heart failure and methamphetamine abuse, *J. Card. Fail.* 26 (3) (2020) 202–209.
- [80] S.X. Zhao, et al., Socioeconomic burden of rising methamphetamine-associated heart failure hospitalizations in California from 2008 to 2018, *Circulation: Cardiovascular Quality and Outcomes* 14 (7) (2021), e007638.
- [81] S.-Y. He, et al., Cardiac muscle lesions associated with chronic administration of methamphetamine in rats, *Am. J. Forensic Med. Pathol.* 17 (2) (1996).
- [82] Y. Maeno, et al., Direct effects of methamphetamine on hypertrophy and microtubules in cultured adult rat ventricular myocytes, *Forensic Sci. Int.* 113 (1–3) (2000) 239–243.
- [83] H. Ito, et al., A comparison of echocardiographic findings in young adults with cardiomyopathy: with and without a history of methamphetamine abuse, *Clin. Cardiol.* 32 (6) (2009) E18–E22.
- [84] S.B. Karch, The unique histology of methamphetamine cardiomyopathy: a case report, *Forensic Sci. Int.* 212 (1–3) (2011) e1–e4.
- [85] M.M. Neeki, et al., Frequency of methamphetamine use as a major contributor toward the severity of cardiomyopathy in adults ≤ 50 years, *Am. J. Cardiol.* 118 (4) (2016) 585–589.
- [86] H.S. Bhatia, et al., Systolic dysfunction in patients with methamphetamine use and heart failure with preserved ejection fraction, *Int. J. Cardiol.* 348 (2022) 90–94.
- [87] J.R. Richards, et al., Methamphetamine use and heart failure: prevalence, risk factors, and predictors, *Am. J. Emerg. Med.* 36 (8) (2018) 1423–1428.
- [88] H. Taegtmeier, S. Sen, D. Vela, Return to the fetal gene program: a suggested metabolic link to gene expression in the heart, *Ann. N. Y. Acad. Sci.* 1188 (2010) 191–198.
- [89] R.A. de Boer, et al., Towards better definition, quantification and treatment of fibrosis in heart failure. A scientific roadmap by the Committee of Translational Research of the Heart Failure Association (HFA) of the European Society of Cardiology, *Eur. J. Heart Fail.* 21 (3) (2019) 272–285.
- [90] N. Ale-Agha, et al., Mitochondrial telomerase reverse transcriptase protects from myocardial ischemia/reperfusion injury by improving complex I composition and function, *Circulation* 144 (23) (2021) 1876–1890.
- [91] Y. Cao, et al., Miro2 regulates inter-mitochondrial communication in the heart and protects against TAC-induced cardiac dysfunction, *Circ. Res.* 125 (8) (2019) 728–743.
- [92] Tsushima, K., et al., Mitochondrial Reactive Oxygen Species in Lipotoxic Hearts Induce Post-Translational Modifications of AKAP121, DRP1, and OPA1 that Promote Mitochondrial Fission. (1524-4571) (Electronic).
- [93] S.M. Graves, et al., Mitochondrial oxidant stress mediates methamphetamine neurotoxicity in substantia nigra dopaminergic neurons, *Neurobiol. Dis.* 156 (2021), 105409.
- [94] V. Bazyljanska, et al., Dopamine and methamphetamine differentially affect electron transport chain complexes and parkin in rat striatum: new insight into methamphetamine neurotoxicity, *Int. J. Mol. Sci.* 23 (1) (2022).
- [95] P. Lenzi, et al., Alterations of mitochondrial structure in methamphetamine toxicity, *Int. J. Mol. Sci.* 23 (16) (2022).
- [96] A. Akki, K. Smith, A.M. Seymour, Compensated cardiac hypertrophy is characterised by a decline in palmitate oxidation, *Mol. Cell. Biochem.* 311 (1–2) (2008) 215–224.
- [97] M.F. Allard, et al., Contribution of oxidative metabolism and glycolysis to ATP production in hypertrophied hearts, *Am. J. Physiol.* 267 (2 Pt 2) (1994) H742–H750.
- [98] F.L. Sheeran, et al., Adaptations in protein expression and regulated activity of pyruvate dehydrogenase multi-enzyme complex in human systolic heart failure, *Oxid. Med. Cell. Longev.* 2019 (2019), 4532592.
- [99] J. Dan Dunn, et al., Reactive oxygen species and mitochondria: a nexus of cellular homeostasis, *Redox Biol.* 6 (2015) 472–485.
- [100] Godar, R.J., et al., Repetitive Stimulation of Autophagy-Lysosome Machinery by Intermittent Fasting Preconditions the Myocardium to Ischemia-Reperfusion Injury. (1554-8635) (Electronic).
- [101] Y. Chen, M.B. Azad, S.B. Gibson, Superoxide is the major reactive oxygen species regulating autophagy, *Cell Death Differ.* 16 (7) (2009) 1040–1052.
- [102] D.J. Klionsky, et al., Guidelines for the use and interpretation of assays for monitoring autophagy (4th edition)1, *Autophagy* 17 (1) (2021) 1–382.
- [103] J. Trnka, et al., A mitochondria-targeted nitroxide is reduced to its hydroxylamine by ubiquinol in mitochondria, *Free Radic. Biol. Med.* 44 (7) (2008) 1406–1419.